A POTENTIAL SHORT-CUT TO QUANTITATIVE MINERALOGY

BY

KUO-PIN TSENG

A THESIS
SUBMITTED TO THE FACULTY OF

ALFRED UNIVERSITY

IN PARTIAL FULFILLMENT OF THE REQUIREMENTS
FOR THE DEGREE OF

MASTER OF SCIENCE

IN

CERAMIC ENGINEERING

ALFRED, NEW YORK

AUGUST, 2015

A POTENTIAL SHORT-CUT TO QUANTITATIVE MINERALOGY

BY

KUO-PIN TSENG

B.S. NATIONAL CHENG KUNG UNIVERSITY (2011)

SIGNATURE OF AUTHOR_____

APPROVED BY_____
WILLIAM M. CARTY, ADVISOR

_____
DOREEN D. EDWARDS, ADVISORY COMMITTEE

_____
DAWEI LIU, ADVISORY COMMITTEE

_____
CHAIR, ORAL THESIS DEFENSE

ACCEPTED BY_____
DOREEN D. EDWARDS, DEAN
KAZUO INAMORI SCHOOL OF ENGINEERING

ACKNOWLEDGMENTS

I would like to express my gratitude to my thesis committee members, Dr. Doreen Edwards and Dr. Dawei Liu, for their support and their dialogues regarding this project; and my deepest gratitude to my advisor, Dr. William Carty for his advice, assistance and patience with this project. I enjoyed the time spent together assessing different possibilities of methods and problem solving. He has helped me to think critically throughout this process and is always an encouragement. It was under his guidance that I had the opportunity to deliver my first paper at the 2015 American Ceramic Society in St. Louis Section and Refractory Ceramics Division, USA. It has been a great honor to work with him and I am proud to have been his student.

Thank you to Dr. Xiuhong Du for her assistance in solving mathematical problems. I would also like to thank Hyojin Lee, David Crenshaw, James Thiebaud, Terry Guild and Mirela Dragan for their help in the technological department. Thank you to Yan Yang, Aubrey Fry, Jon Wang, Krishna Amin, Katie Decker, Trevor Riley and my sister, Ayung Tseng, for your help reviewing this thesis. I would also like to thank my friends—Ruifeng Ouyang, Wirat Lerdprom, Victor Colorado, Kevin Keefe, Nick Rozard, Max Modugno, Kirsten Fuller, Kathryn Tierney, Sureeporn Chothirawat, Yiyu Li, Peng Gao, and Wei Zhang for their companionship and making life in Alfred colorful. Finally, a special thanks to my family for their unconditional love and support during my Master's study.

Kuo-Pin (David) Tseng

Alfred, NY—August 2015

TABLE OF CONTENTS

LIST OF TABLES

Page

LIST OF FIGURES

ABSTRACT

Quantitative mineralogy is a critical aspect of material performance and is typically obtained via quantitative X-ray diffraction (QXRD). This thesis proposes that quantitative mineralogy can be reasonably predicted from readily measured material properties (such and density and coefficient of thermal expansion) using a volume based rule of mixtures (ROM) approach. Obtaining the mineralogy of a two-component system is straightforward from a single property, but to obtain the mineralogy of a three-component system requires two property measurements. It should also be possible to use the starting chemistry as a constraint if the chemical reactions and resulting reaction products are simple. The ROM approach has two initial restrictions: (1) the difference of component property values should be significantly different, (2) the properties of different phases should not increase consistently. Other restrictions are possible, with the most obvious being the potential contribution of anisotropy.

Three systems were evaluated to determine feasibility of this approach: porcelain, mullite, and spinel. The predicted mineralogy was compared to results obtained using QXRD via an internal standard method. Results show that the predictions based on ROM approach match the QXRD results with approximately a 95% confidence. It is proposed that this approach may predict the mineralogy of systems composed of more than three components (n=3) using n-1 measured properties or constraints (such as chemistry).

I. INTRODUCTION

Determining mineralogy by a Quantitative X-ray Diffraction (QXRD) method is an expensive, complicated and laborious process. Using the internal standard method, the sample and additive standard require randomly oriented fine powder and a lengthy scanning time. Furthermore, QXRD involves pattern modeling through powerful yet expensive analytical software.[1] An alternative approach to determine mineralogy via the concept of Rule of Mixture (ROM) can be done by simple property measurements.

ROM on a volume fraction basis can be used to calculate material properties, e.g., density, coefficient of thermal expansion, etc.[2-4] However, reversing this route to predict the mineralogy has not been addressed. Compared to QXRD that obtained the compositions for each phase by an additive standard, this approach directly estimates the mineralogy information for each phase with a simple procedure.

In this approach, properties were measured to predict mineralogy for ternary systems. The theory will be introduced then validated by three systems of experiments (mullite, porcelain and spinel synthesis). Results indicate that the predictions based on physical properties have the average error less than 5% compared with mineralogy data collected via QXRD. The accuracy of this method depends on the accuracy of each measurement and the property magnitude of each mineral phase. Specifically, the larger the difference between the component properties, the greater the possible precision for predicting mineralogy. Furthermore, this ROM method can also diagnose the existence of impurity phases if no result can be found in predicted mineralogy. Two properties, density and coefficient of thermal expansion, are chosen to predict a sample with three components.

Other properties of ROM (elastic modulus, thermal and electrical conductivity, etc.) also have their potential to be used in this method with well understanding of

the parameters (e.g. porosity, microstructure) which will affect the measurement values.

II. BACKGROUND

A. Rule of Mixture

Rule of Mixture (ROM) is commonly used in prediction of properties, such as density, coefficient of thermal expansion (C.T.E.), elastic modulus, shear modulus, etc.[2,5-7] Those properties can be calculated mathematically via the properties of independent phases and their volume fractions.

For example, the density of the sample, ρ_S, is the volume fraction of each phase times the density of that phase:

$$(f_{1,v} \cdot \rho_1) + (f_{2,v} \cdot \rho_2) + (f_{3,v} \cdot \rho_3) + \cdots + (f_{n,v} \cdot \rho_n) = \rho_S \quad (1)$$

Where

$$f_{1,v} + f_{2,v} + f_{3,v} + \cdots + f_{n,v} = 1 \quad (2)$$

A similar relationship can be written for C.T.E.:

$$(f_{1,v} \cdot CTE_1) + (f_{2,v} \cdot CTE_2) + (f_{3,v} \cdot CTE_2) + \cdots + (f_{n,v} \cdot CTE_n) = CTE_S \quad (3)$$

If a mass fraction basis is used then the specific volume ($\upsilon = 1/\rho$) is used instead of density:[4]

$$(f_{1,m} \cdot \upsilon_1) + (f_{2,m} \cdot \upsilon_2) + (f_{3,m} \cdot \upsilon_2) + \cdots + (f_{n,m} \cdot \upsilon_n) = \upsilon_S \quad (4)$$

In an intimate mixture of two-mineral phases, the specific volume can be plotted as a linear relationship with a different mass fraction of one component (Figure 1). However, the relationship for densities between two phases under mass fraction can be plotted as a curve (Figure 2), which the linear density relationship between two components need to be calculated under a volume fraction basis (Figure 3). In this system, the mineralogy of two components can be estimated easily via density or other ROM properties.

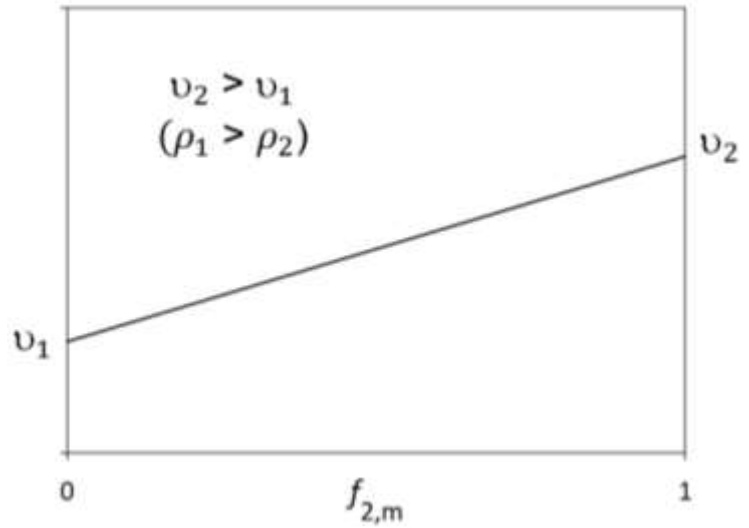

Figure 1. Theoretical specific volume for a two-phase mixture under mass fraction basis.

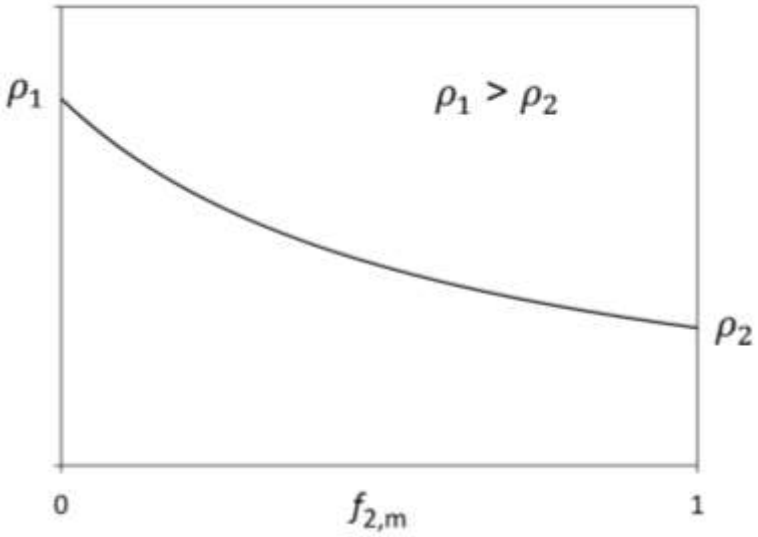

Figure 2. Under mass fraction basis, the relationship of densities in a two-phase mixture can be presented as a curve.

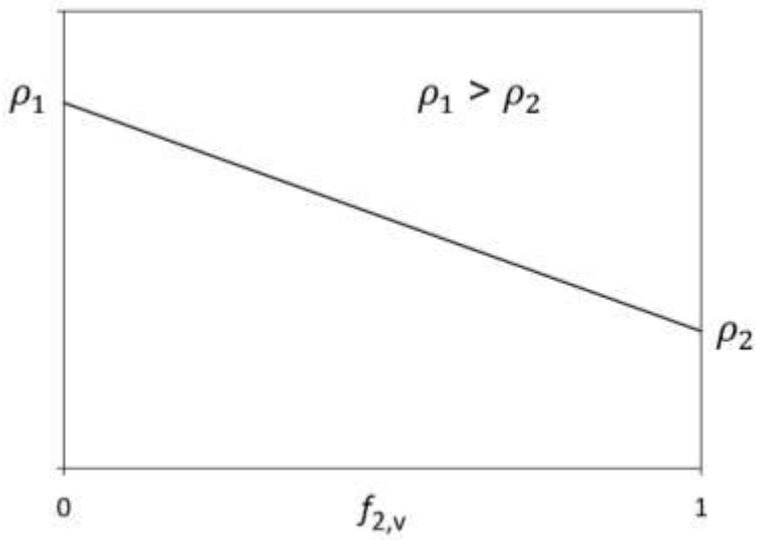

Figure 3. The linear relationship of densities between two components can be made under volumetric fraction basis.

This study focuses on how to depend on this basic idea and extend it to predict mineralogy of three-component materials. Mineralogy with three phases is presented on a ternary diagram, with each vertex of triangle represent 100% composition for each phase. Based on the nature of Rule of Mixture, each value of physical properties can be plotted on a volumetric ternary diagram under a linear relationship. On Figure 4, each solid blue line represents one specific value of the property. The gradient of properties for three components, A, B and C, can be C>A>B or B>A>C. Furthermore, the triaxial diagram follows the rule that the ratio of two components is constant on any line that extends from the third corner, as illustrated in Figure 5. In the beginning of this study, it was hypothesized that by measuring the density of a specimen, a second density measurement obtained by spiking the sample with one of the components, would have a constant ratio of other two components. By combining these two measurements, the ratio of the other two components could be deduced and by extrapolation the overall mineralogy of the original specimen uniquely determined.

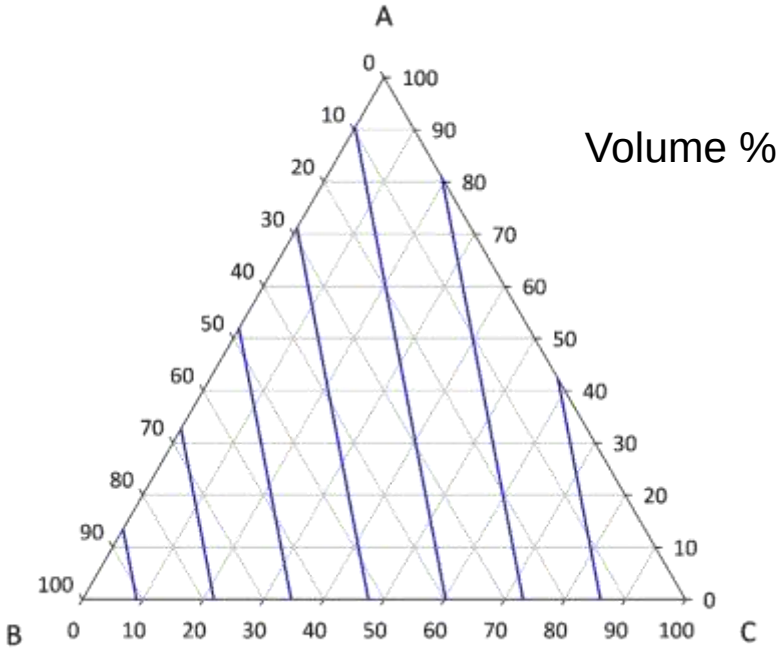

Figure 4. The property values which followed ROM can be plotted as a linear line on Ternary diagram. The gradient of this property can be C>A>B or B>A>C.

$$\frac{a}{b} = \frac{a_1}{b_1} = \frac{a_2}{b_2}$$

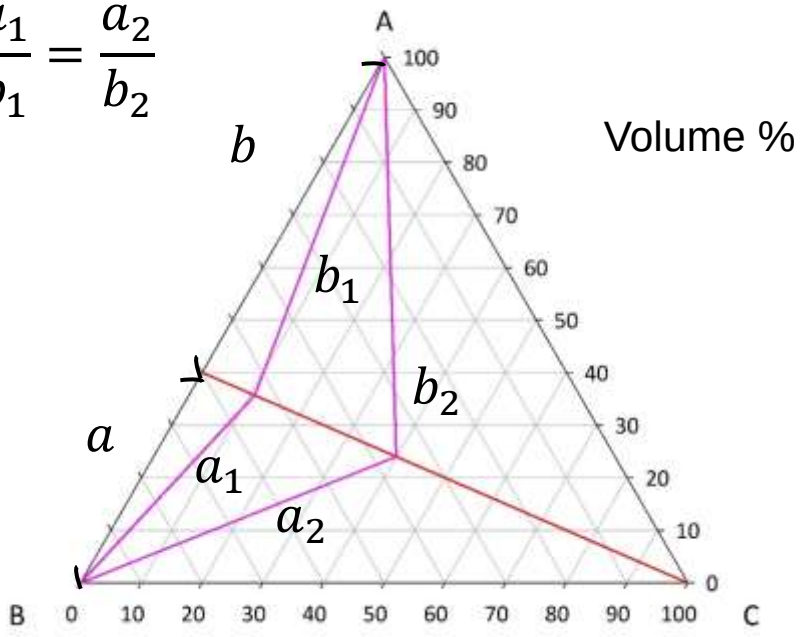

Figure 5. The ratio of two components (A&B) is constant on any point of the red line that extends from the third component (C).

From the measured densities of original specimen and the sample after spiking with component C, all possibilities of the a/b ratio can be represented in the gray area (Figure 6). The main factor of this approach is to find the interval between two samples. Despite different interval represents to different a/b ratio, the difference between those intervals is small. Furthermore, the composition of spiking material need to be calculated under volume fraction basis. Conceptually the idea is valid but practically a unique solution was not obtained due to the precision of the density measurement; even small error of measurements can vary the interval as well as a/b ratio. This result is verified using experimental calculations and indicated that it is not possible to obtain the mineralogy from density measurements alone.

A.

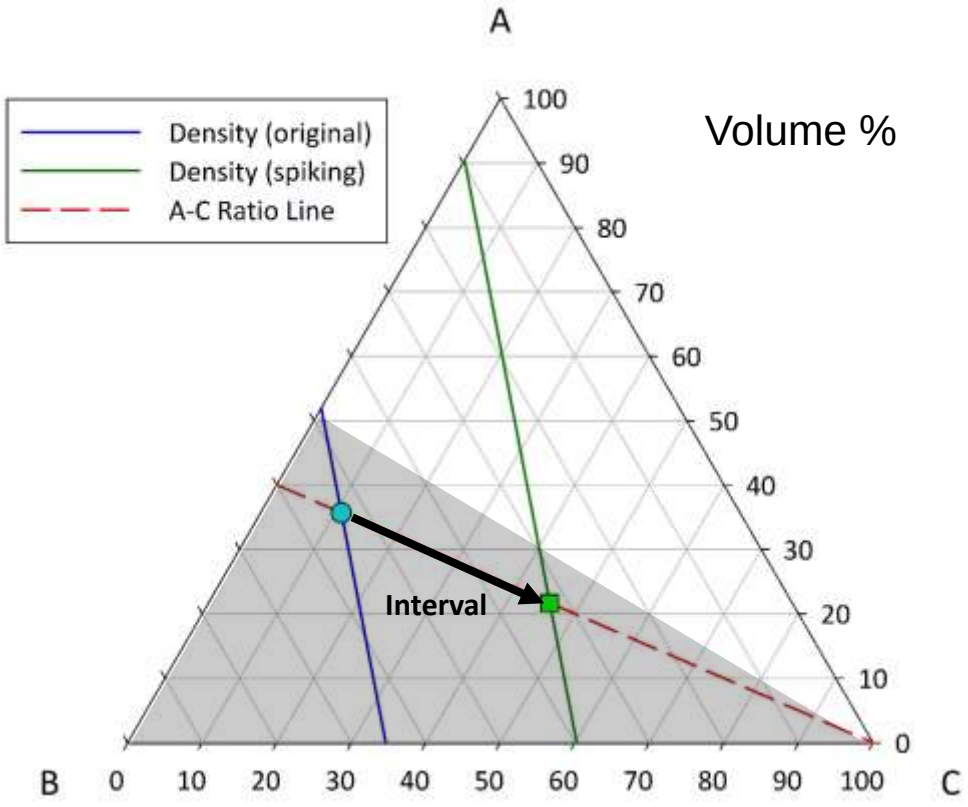

B.

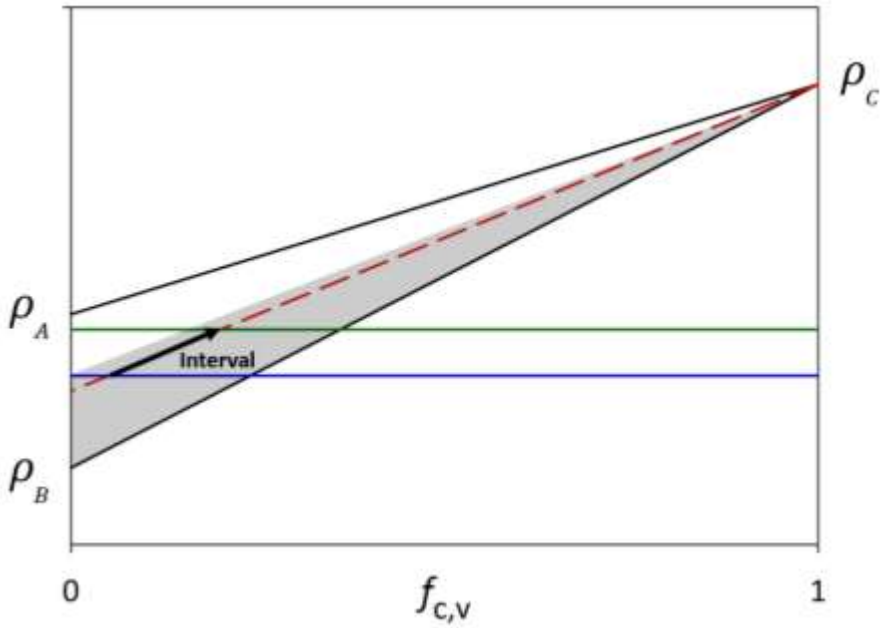

Figure 6. With the original density and the density after spiking measured, the possible a/b ratio is shown in the gray area on the ternary diagram. The red dash represents one possible a/b ratio under this range. In order to get the correct a/c ratio, the interval level of the spiking material must be obtained.

An alternative approach is proposed that more material properties follow the Rule of Mixture can be used in calculation. From the nature of volume fraction in Equation (2), the mineralogy of materials with three unknown components still need to be solved using two other equations; therefore, two additional properties need to be measured. In order to predict mineralogy, the relationship between the number of phases in the material and the properties measured is listed in Table I.

Table I. The Requirement of Number of Properties Needed in order to Predict in Multi-phase Materials

Number of phases	Number of ROM properties required	Example
2	1	Density (ρ)
3	2	ρ + C.T.E.
4	3	ρ + C.T.E. +starting chemistry (under simple reaction)

After obtaining the values of two properties, the predicted mineralogy could be shown on a triaxial diagram. Figure 7 shows the gradient of the first property (solid line) among three components can be C>B>A or A>B>C and the second property (dash line) can be C>A>B or B>A>C. From these measurements, the intersection of two properties (green and red lines) on the ternary diagram is the mineralogy for the sample on a volume fraction basis. Since each measurement may vary slightly, there is a hypothesis that the three components need to have significantly different property values. The larger the difference between the component properties, the greater the accuracy for predicting the mineralogy; that is to say, larger differences between the component properties provide larger tolerance on the deviation from repeated measurements. In order to increase the precision of mineralogy, a second requirement is that the properties should not increase consistently, as illustrated in Figure 7. Otherwise, the slight difference in

the measured property would significantly offset the predicted mineralogy. Another approach is to predict the mineralogy via one property measurement and starting chemistry.

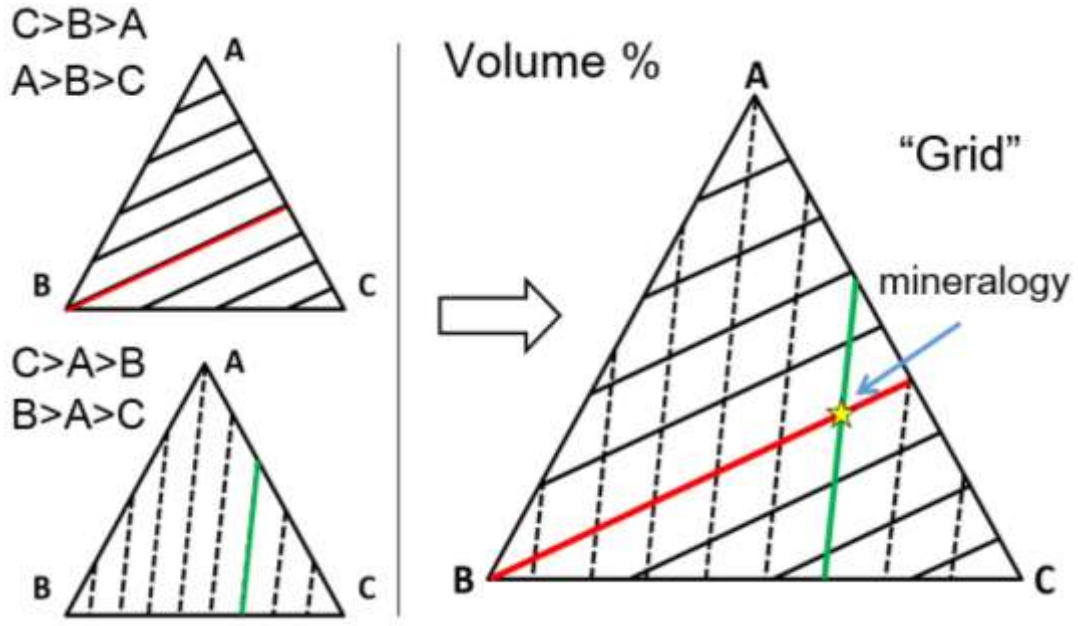

Figure 7. The "grid" ternary diagram can be made via two properties followed ROM under volume fraction. After measuring two properties (red and green line), the mineralogy of a three-component sample can be determined.

1. Mineralogy predicted by two measured properties

The mineralogy of three-component materials can be predicted via two properties (p_a & p_b). From the Equation (1), the properties of sample follow the relations:

$$\left(f_{1,v} \cdot p_{1,a}\right) + \left(f_{2,v} \cdot p_{2,a}\right) + \left(f_{3,v} \cdot p_{3,a}\right) = p_{S,a} \quad (5)$$

$$\left(f_{1,v} \cdot p_{1,b}\right) + \left(f_{2,v} \cdot p_{2,b}\right) + \left(f_{3,v} \cdot p_{3,b}\right) = p_{S,b} \quad (6)$$

The sum of the volume fraction is one under a three-component system.

$$f_{1,v} + f_{2,v} + f_{3,v} = 1 \quad (7)$$

From the three equations above, the volume fraction of each phase can be calculated through Cramer's rule:[8]

$$\begin{bmatrix} 1 & 1 & 1 \\ p_{1,a} & p_{2,a} & p_{3,a} \\ p_{1,b} & p_{2,b} & p_{3,b} \end{bmatrix} \begin{bmatrix} f_{1,v} \\ f_{2,v} \\ f_{3,v} \end{bmatrix} = \begin{bmatrix} 1 \\ p_{m,a} \\ p_{m,b} \end{bmatrix} \tag{8}$$

$$f_{1,v} = \frac{det\begin{bmatrix} 1 & 1 & 1 \\ p_{m,a} & p_{2,a} & p_{3,a} \\ p_{m,b} & p_{2,b} & p_{3,b} \end{bmatrix}}{det\begin{bmatrix} 1 & 1 & 1 \\ p_{1,a} & p_{2,a} & p_{3,a} \\ p_{1,b} & p_{2,b} & p_{3,b} \end{bmatrix}} \tag{9}$$

$$f_{2,v} = \frac{det\begin{bmatrix} 1 & 1 & 1 \\ p_{1,a} & p_{m,a} & p_{3,a} \\ p_{1,b} & p_{m,b} & p_{3,b} \end{bmatrix}}{det\begin{bmatrix} 1 & 1 & 1 \\ p_{1,a} & p_{2,a} & p_{3,a} \\ p_{1,b} & p_{2,b} & p_{3,b} \end{bmatrix}} \tag{10}$$

Where $p_{m,a}$ and $p_{m,b}$ represent to a and b properties measured. And therefore, the third component is given by,

$$f_{3,v} = 1 - (f_{1,v} + f_{2,v}) \tag{11}$$

From these calculations, the mineralogy of three phases can be obtained. As shown in the triaxial diagram (Figure 7), the result is the intersect point between measured properties.

2. Mineralogy predicted by one measured property with starting chemistry

The second method can be used if the reaction is straightforward: the starting chemistry provides a reaction chemistry constraint. The final mineralogy can be calculated by chemical reactions from the starting chemistry and the reaction route can be plotted on the ternary diagram, as shown in Figure 8. The stoichiometric chemistry of A and B components can be fully reacted to C component as a final mineralogy. With less phase B as the raw material, the final mineralogy will contain

both A and B phases. On the other side, compared to stoichiometric starting chemistry, the final mineralogy of component C and excessive B can be formed from the reaction of smaller amount of phase A as starting material.

The chemistry route between a green body and fully reacted material, represented by adjacent sides on the triaxial diagram, can be addressed as following equation:

$$f_{1,2,3} = G_{1,2,3} + a\left(U_{1,2,3} - G_{1,2,3}\right) \quad (0 \le a \le 1) \tag{12}$$

Where f is the composition for each phase, which is calculated from raw materials, G is the original composition for each phase, and U is the ultimate mineralogy. Parameter a is the number between 0 and 1, which represents to the mineralogy of starting and final mineralogy. The final composition will be reached after the reaction is totally completed ($a = 1$).

As the first theory, the property measured can be plotted as a linear line on the ternary diagram. This line on the ternary diagram can be represented as:

$$f_{1,2,3} = E_{1,2,3} + b\left(S_{1,2,3} - E_{1,2,3}\right) \quad (0 \le b \le 1) \tag{13}$$

Where S is the mineralogy from one leg, and E is the chemistry composition from the other leg. Parameter b is the number between 0 and 1, which represents to the different mineralogy with the same property.

After combining the Equation (12) and (13), the parameter a and b can be obtained. The mineralogy of the material can be fixed to one point which is the intersection of the chemistry constraint and measured property (Figure 8).

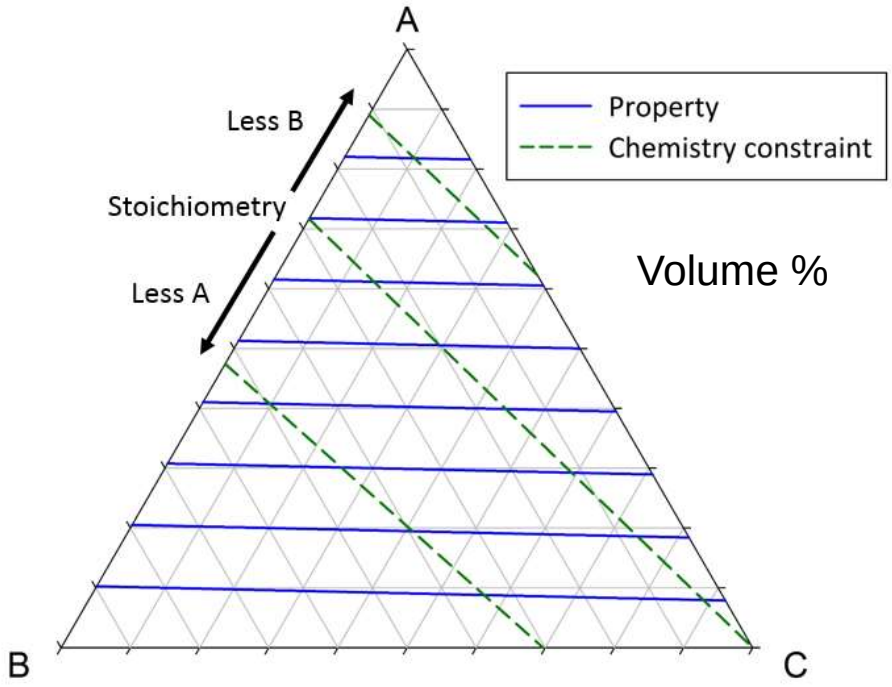

Figure 8. The mineralogy (intersection) can be predicted by starting chemistry and a measured property.

B. Properties

Despite there being several properties following the Rule of Mixture theoretically, some properties like elastic modulus and conductivity are sensitive to porosity or microstructure which make it difficult to get the accurate measurement values from ROM calculations. Properties such as density and C.T.E. with proper sample preparation are independent to microstructure and porosity. As a result, these two properties are ideal candidates to demonstrate the feasibility of this approach.

Density

Density can be measured to high precision. However, the closed porosity increases the sample volume, which decreases the value of measured density. In order to obtain the true density, closed pores must be eliminated. If the volume of the closed pores can be measured, porosity can also be calculated by a ROM

equation with its density value equal to zero (Equation 14).

$$\left(f_{1,v} \cdot \rho_1\right) + \left(f_{2,v} \cdot \rho_2\right) + \left(f_{3,v} \cdot \rho_3\right) + \cdots + \left(f_{n,v} \cdot \rho_n\right) + \left(f_{pores,v} \cdot 0\right) = \rho_S \qquad (14)$$

Thermal Expansion Coefficient

The coefficient of thermal expansion is often referred to as the mean linear C.T.E. under a given temperature range.[9] Materials like mullite and quartz are anisotropic. Therefore, if those phases in sample are aligned/oriented could alter the C.T.E. value from measurement. In this approach, slip casting is used to prepare green body which each components can be randomly oriented in the sample. The second issue may offset the measured C.T.E. value is the large difference of elastic modulus between components, as shown in Equation 15.[10]

$$\alpha = \frac{\sigma}{E \cdot \Delta T} \qquad (15)$$

where α is the coefficient of thermal expansion, E is the elastic modulus and σ is stress. Impurity is another problem which can shift both C.T.E. and density from the actual value. The requirements of these two properties in the ROM approach is listed in Table II.

Table II. The Requirements for Properties in ROM Approach

	Density	C.T.E.
Prediction of three phases	✓	✓
Follow ROM under volume fraction basis	✓	✓
No impurity contained	✓	✓
No closed porosity	✓	
No preferred orientation		✓
Minor affected from elastic modulus		✓

Table III lists the properties for phases which are used in this study. The C.T.E. values are chosen from temperatures ranging 200°C-500°C. For anisotropic materials (mullite, corundum and quartz), the C.T.E. values are obtained from the samples which preferred orientation is assumed to be absent.

Table III. Physical Properties Used in Three Systems

	Density[11,12] (g/cm^3)	C.T.E.[11,13] ($x10^{-6}/K$)	Elastic modulus[14] (GPa)
Mullite*	3.17	4.7	143.1
Corundum*	3.97	8.0	408.8
Quartz*	2.65	23	94.5
Glass	2.39	4.9	64.4
Periclase	3.58	13.5	230.3
Spinel	3.60	7.6	250.7
Cristobalite	2.32	14.5	-

*Anisotropic: C.T.E. are obtained from samples assumed absent of preferred orientation.

C. Experimental approach

Three different synthesis systems: porcelain, mullite, and spinel, are used to verify the availability of ROM approach in predicting three-component mineralogy.

Porcelain

A porcelain body is synthesized from clay, feldspar and quartz. A typical porcelain body contains three phases after sintering temperature above 1200^{o}C: mullite, glass and quartz.[15] Under a temperature range of 1200^{o}C-1500^{o}C, the mineralogy of mullite phase is constant while the quartz dissolved into the glass phase. Extensive experimental work over the past decade has demonstrated that the mullite concentration is constant for any given composition over the noted temperature range and that the mineralogy is independent of heating rate but scales linearly with temperature and with the log scale of dwell time.[16,17] Above 1400^{o}C, the porcelain body is composed of mullite, glass and small amount of quartz.[18,19]

It is proposed that the composition of the glass phase will fall on a “glass formation boundary” (Figure 9).[18] On the ternary diagram, the glass formation boundary is a line with a consistent ratio of alumina to flux under a temperature range 1150^{o}C to 1500^{o}C.[20,21] It was proposed that 1.19$\pm$0.1 (normalized molar basis) of alumina to flux dissolves in the glass phase while excess alumina transforms into mullite.[22] The properties of the glass phase such as C.T.E. and density values are addressed by Skovira’s research.[11] The average thermal expansion coefficient for the glass phase is 4.88$\pm$0.9$\cdot$10^{-6}/K under temperature range 200^{o}C-500^{o}C and average density is 2.39$\pm$0.02 g/cm^{3}. These values of properties do not change significantly during porcelain formation. The C.T.E. values of mullite and the porcelain glass phases are nearly identical, therefore the C.T.E. property of a porcelain body is dominated by the concentration of undissolved quartz.[11]

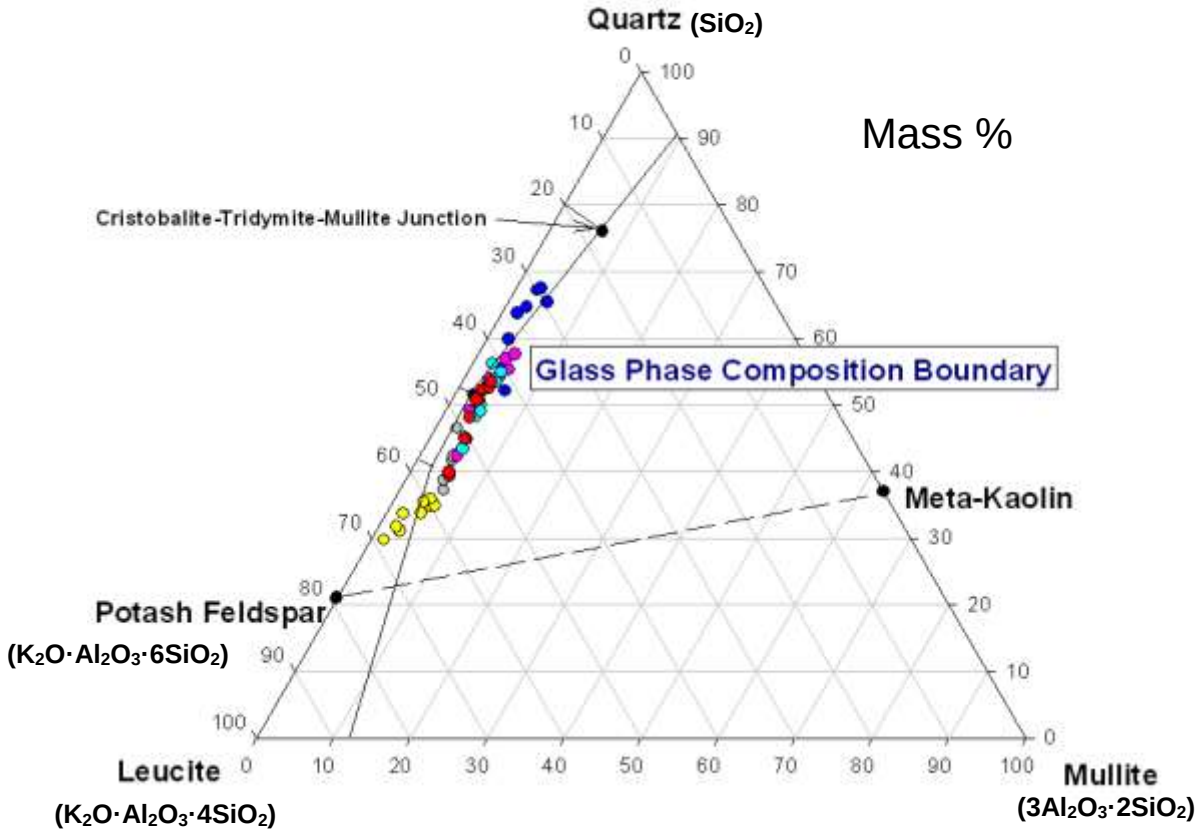

Figure 9. The glass phase composition boundary can be shown on the K_2O-Al_2O_3-SiO_2 ternary diagram.[18]

Mullite

There are different routes to form mullite ($3Al_2O_3 \cdot 2SiO_2$), such as Alumina/Silica or Clay/Alumina as the raw material. Using alumina and silica as the raw materials in mullite formation requires high sintering temperatures for mullitisation (1600°C-1700°C).[23] Even reducing the particles size below 2μm to decrease the sintering temperature, the mullitisation temperature (1400°C) is still high compared to a Clay/Alumina route. As the result, clay like kaolinite ($Al_2O_3 \cdot 2SiO_2 \cdot 2H_2O$) is one of the starting materials commonly used in mullite

synthesis, which significantly decreases mullitisation temperature to 1200°C.

From kaolinite chemical composition, the amount of silica is much greater than in mullite. The excessive silica can be combined with additional alumina, which gives the following reaction:

$$3(Al_2O_3 \cdot 2SiO_2) \rightarrow 3Al_2O_3 \cdot 2SiO_{2\ (primary)} + 4SiO_{2\ (amorphous)} \quad (16)$$

$$4SiO_2 + 6Al_2O_3 \rightarrow 3Al_2O_3 \cdot 2SiO_{2\ (secondary)} \quad (17)$$

Primary mullite is synthesized at temperatures around 1200°C (Equation 16). After the temperature rises to 1400°C, the reaction of alumina and silica in glass phase starts to form secondary mullite (Equation 17).[24,25] The property of primary and secondary mullite is considered to be identical. Under the synthesis with nonstoichiometric raw materials, the final mineralogy are composed of mullite and excessive alumina or silica. In this approach, green bodies are sintered before completion of mullite formation: composed of mullite, glass, and corundum phases coexist in the sample.

Spinel

Magnesium aluminate spinel ($MgO \cdot Al_2O_3$) is an attractive refractory material because of its excellent mechanical and thermal properties at elevated temperatures.[26] Through solid state reactions, spinel can be synthesized from magnesium oxide and alumina at high temperatures (>1400°C).[27] The total reaction can be simplified to the reaction below:

$$MgO + Al_2O_3 \rightarrow MgAl_2O_4 \quad (18)$$

Before the spinel formation is completed, magnesium oxide, alumina, and spinel are three major phases which exist after sintering.

III. EXPERIMENTAL PROCEDURE

A. Raw Materials Selection and Chemical Composition

Porcelain

The porcelain data was obtained from a simple composition of 50% clay (EPK, Edgar Minerals, Edgar, FL, USA), 25% silica (Oglebay Norton Industrial Sands, Inc., Glenford, OH, USA), and 25% feldspar (G-200, Imerys Ceramics, Roswell, GA, USA). Samples were heat treated over the temperature range of 1200^{o}C-1500^{o}C (in 100K increments) producing a final mineralogy of mullite, (undissolved) quartz, and glass.

Mullite

Three different approaches were used in mullite synthesis:

1. Kaolinitic clay (SSP: 47.0% SiO_2 + 35.3% Al_2O_3, Imerys Ceramics, Roswell, GA, USA) with alumina (A-10, Almatis Inc., Leetsdale, PA, USA)
2. Silica (Oglebay Norton Industrial Sands, Inc., Glenford, OH, USA) with alumina (A-10, Almatis Inc., Leetsdale, PA, USA)
3. Colloidal Silica (Ludox TM-50, Sigma-Aldrich, St. Louis, MO, USA) with alumina (A-10, Almatis Inc., Leetsdale, PA, USA)

These raw materials was blended with calcined alumina at three weight ratios: 42%, 52% and 62% alumina (balanced with the other raw materials) bracketing 3:2 stoichiometry. Samples were heat-treated over a temperature range of 1200^{o}C to 1500^{o}C (in 50K increments).

Spinel

Magnesium aluminate spinel ($MgAl_2O_4$) was produced by the reaction of 60% alumina (A-10, Almatis Inc., Leetsdale, PA, USA) with 40% high purity magnesium oxide (Martin Marietta Corp., Bethesda, MD, USA). The green bodies are heat-treated to form spinel at temperatures ranging from 1450°C-1600°C (in 50K increments). This simple reaction follows that one mole of each alumina and magnesium oxide, can synthesize one mole of spinel. The final mineralogy of this spinel synthesis can be calculated as 16.28% excessive magnesium oxide with 83.72% spinel.

The results of the chemical analysis measured for all the raw materials used are listed in Table IV.

Table IV. Measured Chemical Composition of the Raw Materials (Wt. %)

	SiO_2	Al_2O_3	Fe_2O_3	MgO	CaO	Na_2O	K_2O	TiO_2	LOI
EPK	49.44	35.46	0.78	0.17	0.15	0.11	0.45	0.45	14.21
Silica	98.96	0.41	0.05	0.01	0.02	0.14	-	0.01	0.39
G-200	67.28	17.64	0.06	0.01	0.09	2.85	10.86	0.01	1.20
SSP	47.00	35.29	0.42	0.21	0.06	0.20	1.16	0.03	15.43
A-10	-	98.87	-	0.01	0.03	0.32	-	-	0.77
MgO	0.40	0.10	0.20	98.20	0.90	-	-	-	0.20

Sample preparation and characterization

All samples were prepared by slip casting in gypsum molds and were fired in air in a $MoSi_2$ furnace (DT-31-RS-14, Deltech Inc., Denver, CO, USA) at a heating rate of 5K/min with one hour dwelling time. After heat treatment, specimens were cut for C.T.E. measurements and crushed to pass a 325-mesh screen for density measurements using a Helium-pycnometer (Accupyc 1330, Micrometrics Instrument Corp., Norcross, GA, USA). After density measurements, the powder was mixed with 10 wt. % CaF_2 as an internal standard for QXRD measurement.

B. Analyses

1. Helium pycnometer

Density was measured using a Helium-pycnometer (Accupyc 1330, Micrometrics Instrument Corp., Norcross, GA, USA) at room temperature. The calibration balls are used to correct the pycnometer before experiments. Closed pores inside particles occupied the sample volume thus lower the density measured. The relationship of powder density with different grain size is shown in Figure 10. The blue line in figure represents density calculated through ROM by mineralogy. The large particles with more closed pores inside the grains significantly decrease the measured density. After total particle size was smaller than 53μm via passing through a 270 mesh sieve, the occupation of closed porosity was eliminated and the measured density is similar to the one calculated from ROM. The samples from each system (mullite, porcelain, and spinel) were examined using a scanning electron microscopy (Quanta 200F, SEM, FEI Co., Hillsboro, OR, USA). From SEM images with powder passed through 40 mesh sieve (425μm) and 140 mesh sieve (105μm), pores are exposed outside the grains, and it is possible that closed pores can be in those grains (Figure 11-13 AB). From the image for powders passing through 325 mesh sieve (44μm), those grains are small enough and there is no smaller pores exposed outside (Figure 11-13 C), thus it can be considered as sample without closed porosity. Furthermore, the measured densities with samples passing through 270 mesh sieve remain constant which indicate that all the closed porosity can be eliminated if particle size is small enough. Three measurements were taken of each sample and average density of these measurements were calculated for analysis.

The reliability of Helium pycnometer is ±0.0018 g/cm^3, tested by ten measurements on high purity alumina (AKP-50, Sumitomo Chemical Co., Ltd., Japan).

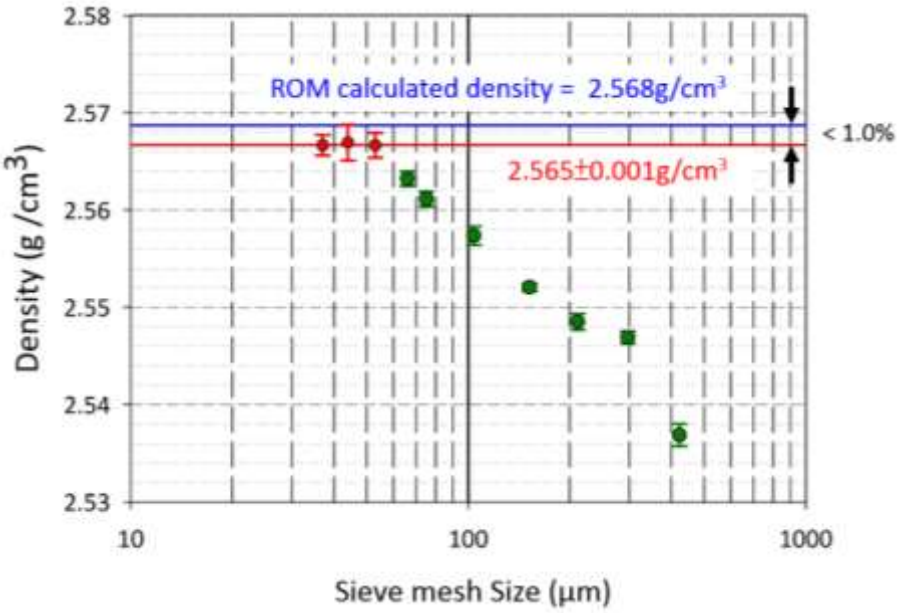

Figure 10. Measured density can be lower from testing larger particle with closed porosity inside, which increase the volume of sample. After particle size smaller than 53µm (red plot), the error between measured and calculated densities is less than 1.0%.

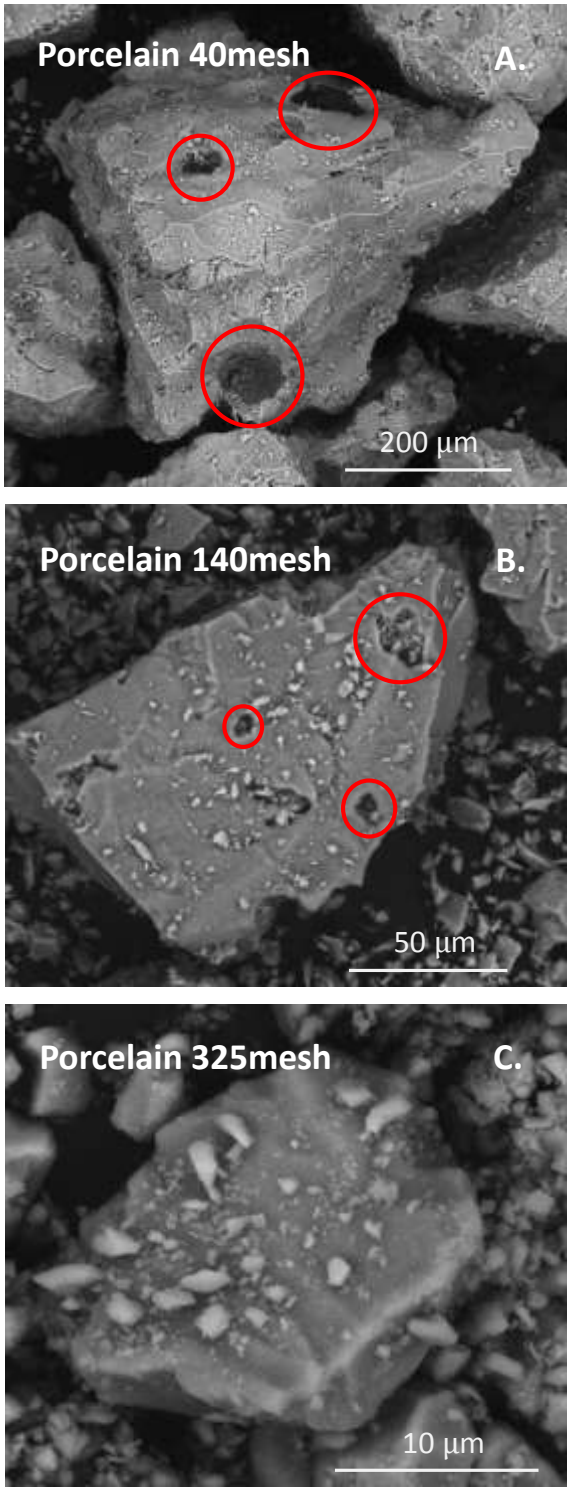

Figure 11. The SEM images show no exposed porosity after porcelain powder passes through 325 mesh sieve (44µm). The exposed closed pores can be found on the surface of particles after pass through 40 and 140 mesh sieves with mesh size 425 and 105 µm respectively.

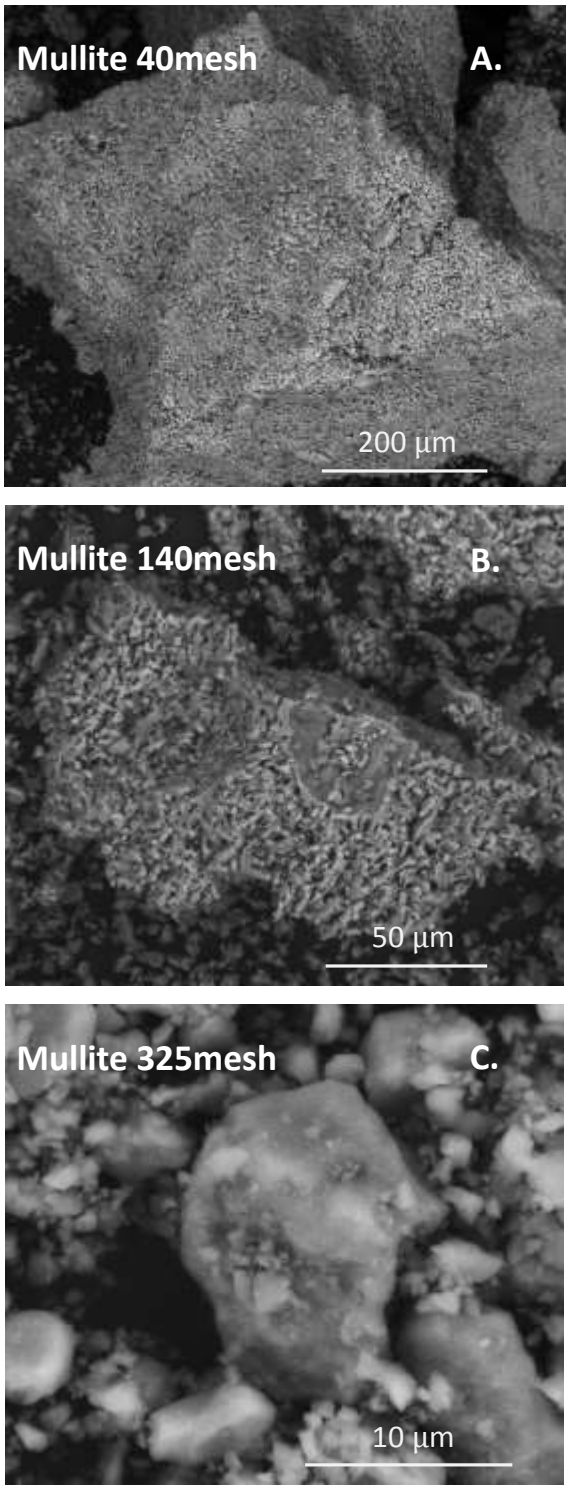

Figure 12. The SEM images show no exposed porosity after mullite powder passes through 325 mesh sieve (44µm). The exposed closed pores can be found on the surface of particles after pass through 40 and 140 mesh sieves with mesh size 425 and 105 µm respectively.

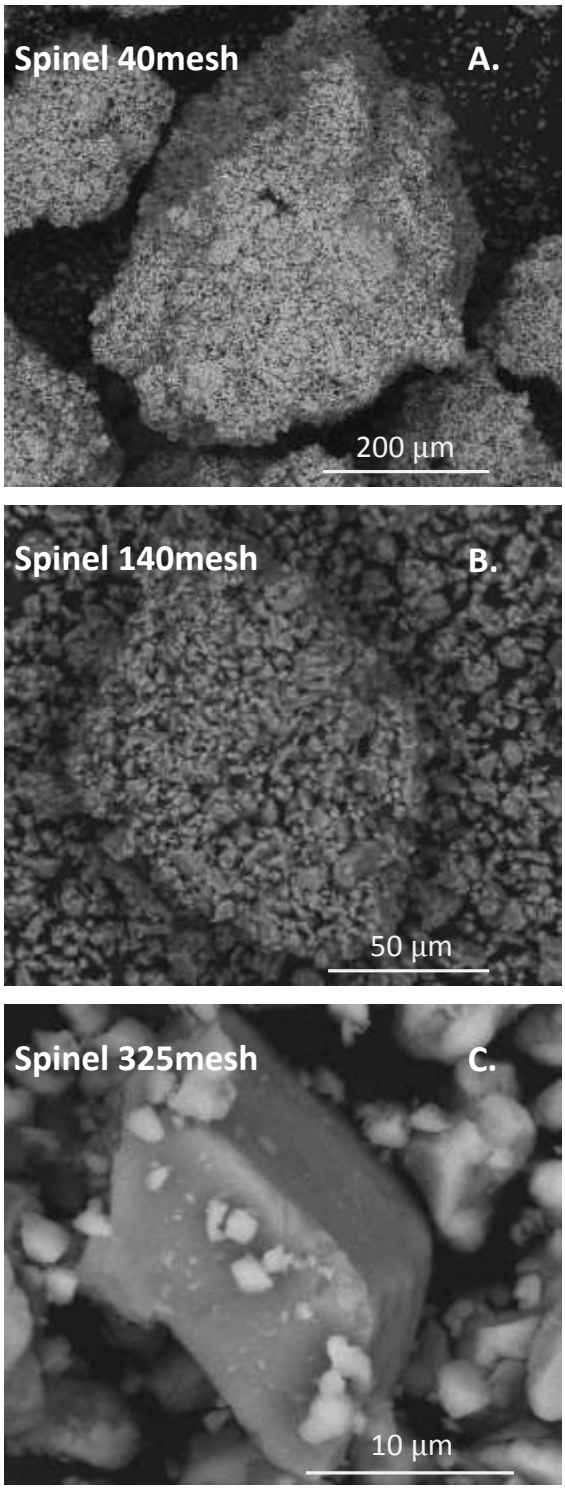

Figure 13. The SEM images show no exposed porosity after spinel powder passes through 325 mesh sieve (44µm). The exposed closed pores can be found on the surface of particles after pass through 40 and 140 mesh sieves with mesh size 425 and 105 µm respectively.

2. Dilatometer

The coefficient of thermal expansion (C.T.E.) was measured in a single push rod dilatometer (Model 1600, Edward Orton Jr. Ceramic Foundation, Westerville, OH, USA). The instrument was calibrated with a 2.54 cm (1.0 inch) high purity alumina standard (Edward Orton Jr. Ceramic Foundation, Westerville, OH, USA). The accuracy of dilatometer is $\pm 0.18 \times 10^{-6}$/K, tested by ten measurements on the same alumina standard.

The samples for C.T.E. measurement were cut in 2.54 ± 0.0025 cm with parallel edges. The heating rate is 5K/min from 34°C to a peak temperature of 1000°C. The linear thermal expansion is calculated by fitting a linear trend line to the percent linear expansion with temperature plot of 200°C to 500°C range for all samples. The linear thermal expansion of a porcelain body (Figure 14) abruptly increased due to the α-β quartz inversion at 573°C. To ensure the accuracy and uniformity for all measurements, the temperature range 200°C-500°C is used for all the samples.

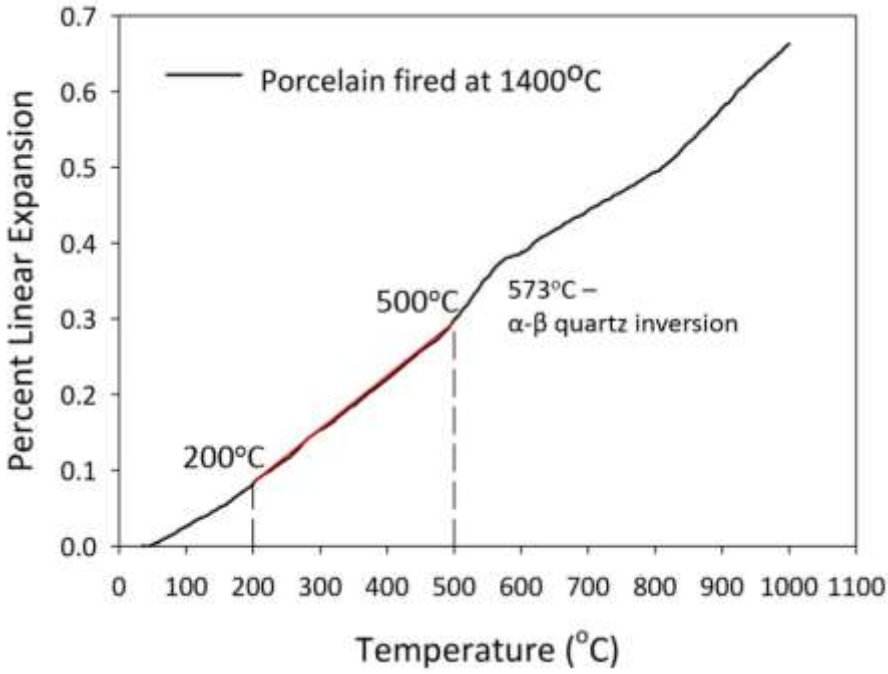

Figure 14. The dilatometer records the percent linear expansion with temperature in porcelain sample. Linear thermal expansion abruptly increased due to the α-β quartz inversion at 573°C. Temperature range 200°C-500°C is used to analysis C.T.E.

3. X-ray Diffraction

Quantitative X-Ray Diffraction analysis was performed using an internal standard method with 10 wt. % CaF_2 as an internal standard. The CaF_2 and the specimen powder were mixed for 15 minutes using a motorized mortar and pestle. Powder diffraction data (Bruker D2 Phaser, Madison, WI, USA) was collected from 15° to 60° (25° to 65° for spinel system) 2θ with CuKα radiation (λ = 0.154 nm) at 30kV and 10 mA with a step size of 0.04° and a count time of four seconds. Diffraction patterns were analyzed using commercial software (*Jade,* v.9, Materials Data Inc. Livermore, CA, USA). Three non-overlapping peaks were selected for most mineral phases and for the CaF_2 standard, listed on Table V. Comparing the total area of the peaks for each phase to that of the CaF_2 standard gives the volume percentage of that phase in the body. The data is corrected for the density of the mineral phases.

Table V. XRD Peaks and Equations for Quantitative Analysis

	2θ and Crystal Orientation			Equation	Reliability (wt. %)*
Mullite	31.0 (001)	33.2 (220)	40.9 (211)	$x = \frac{y + 0.0046}{0.1183}$	±1.0%
Quartz	20.9 (100)	40.3 (111)	50.2 (112)	$x = \frac{y + 0.7200}{0.1850}$	±0.7%
Corundum	37.8 (110)	43.4 (113)	52.6 (024)	$x = \frac{y + 0.0036}{0.0258}$	±1.5%
Cristobalite	31.5 (102)	36.2 (200)	48.6 (212)	$x = \frac{y + 0.0002}{0.1222}$	±1.0%
MgO	42.9 (200)	-	62.3 (220)	$x = \frac{y + 0.3237}{1.3475}$	±1.1%
CaF_2	28.3 (111)	47.0 (220)	55.8 (311)	-	-

* The reliability is relative to the measured value, not absolute.

In these equations, y is the peak area of the phase divided by the peak area of the standard and x is the volume percent of the phase. Those x-values are then corrected for weight percentage of the phase. The composition of the glass phase (in porcelain/mullite system) and spinel phase (in spinel system) are obtained from the balance of the other two phases.

IV. RESULT AND DISCUSSION

A. Porcelain

In porcelain formation, the final mineralogy is composed of mullite, quartz, and glass phases. The properties of a porcelain body follow the requirements for the ROM approach, which the density and C.T.E. values do not increase consistently and the values for each property are significantly different, can be plotted in a triaxial grid diagram (Figure 15).

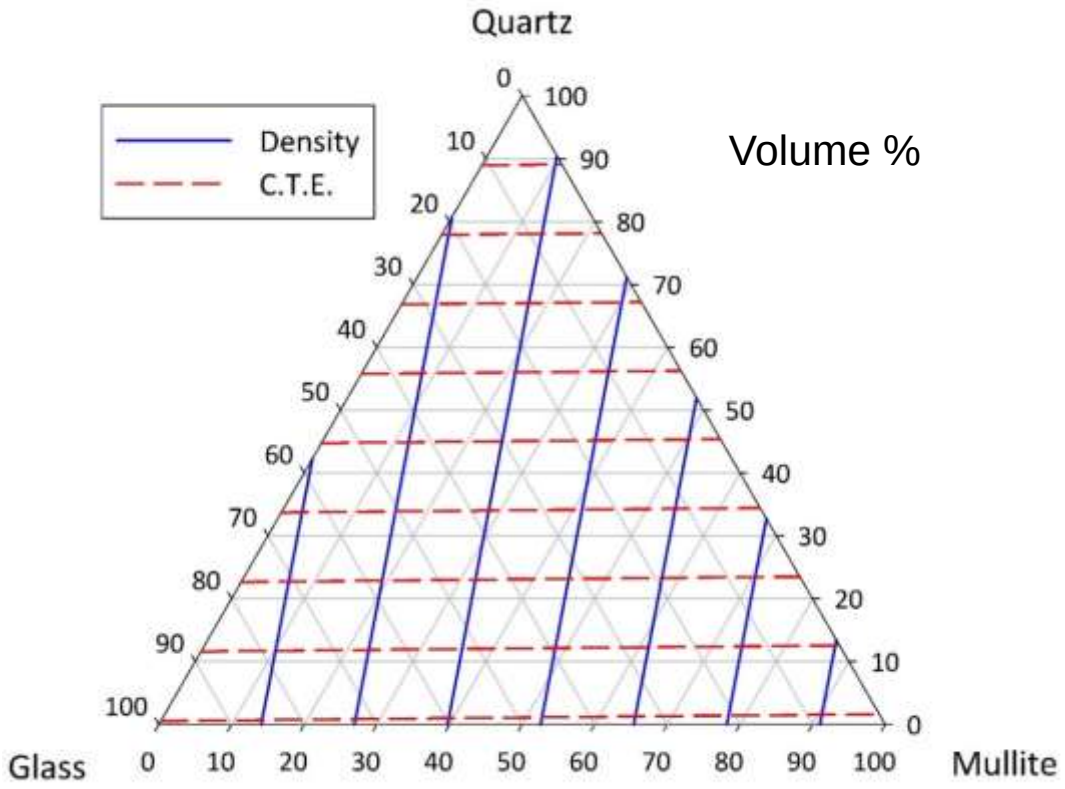

Figure 15. The grid plot for porcelain comparing density and C.T.E.

Figure 16 plots the mineralogy by QXRD analysis. The mullite level (mass %) in porcelain samples is 26.34% ±2.1% indicating that the mullite level is independent of temperature, which is consistent with previous works.[16,20,28] The

amount of glass phase is balance by the fraction difference of mullite and quartz phases.

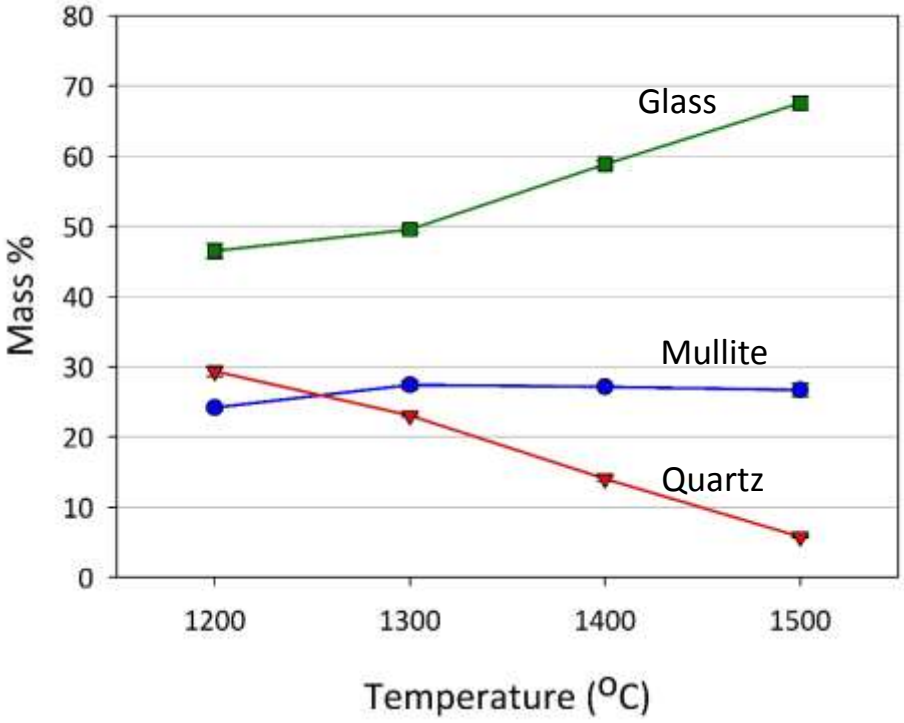

Figure 16. The mineralogy of porcelain samples fired from 1200°C to 1500°C.

The measured and calculated densities and C.T.E. (based on mineralogy analyzed by QXRD) are plotted in Figure 17 and 18 as a function of temperature. The correlation of C.T.E. property is better than density because the difference of C.T.E. values is larger among three components in the porcelain body. The C.T.E. values in the porcelain body is dominated by the quartz phase, which C.T.E. property (23.0 $x10^{-6}$/K) is about 4.8 times greater to the other two compositions.

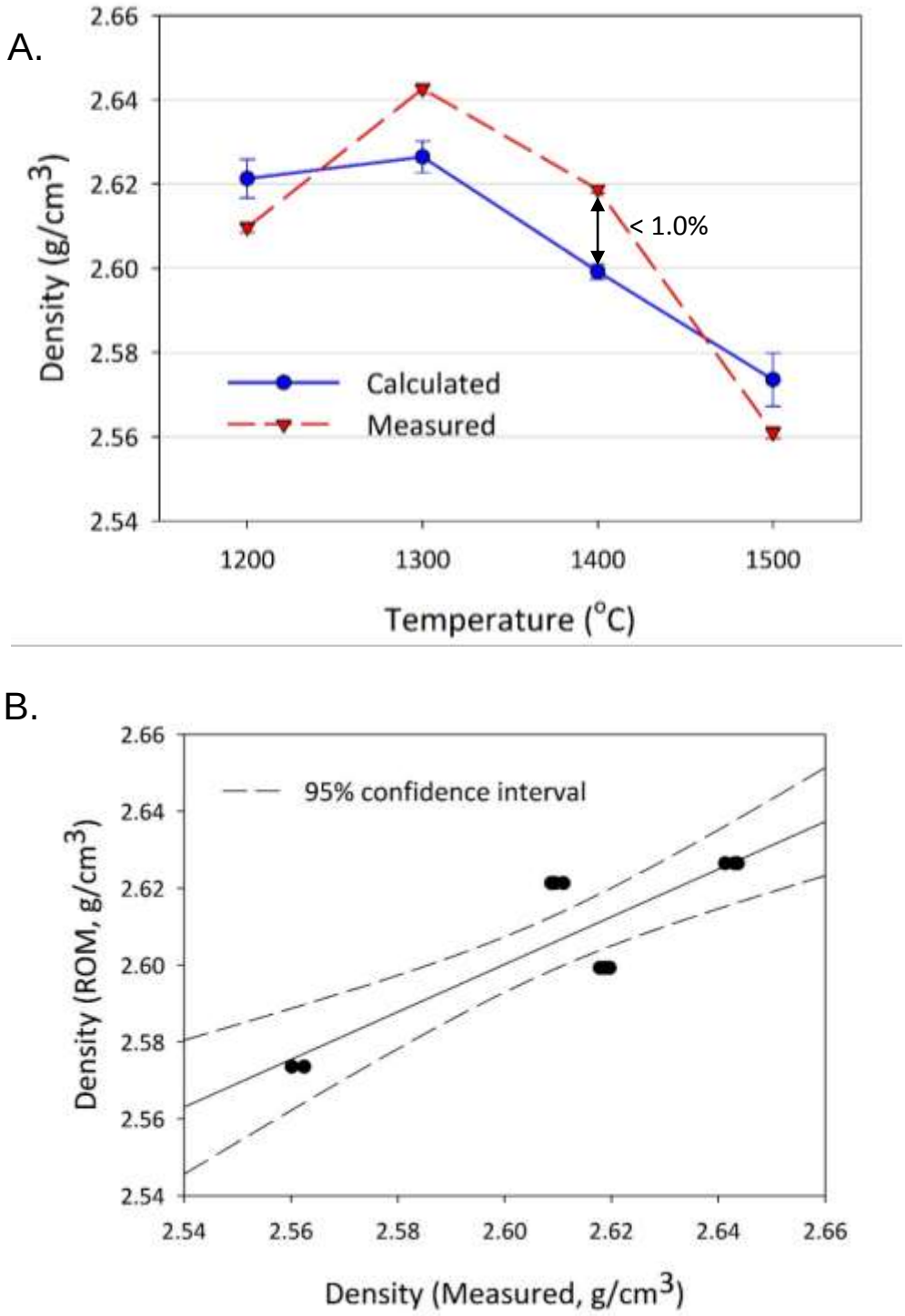

Figure 17. Measured and calculated density values for the porcelain body fired at different temperatures (A). The calculated density values match well with the measured values (B).

A.

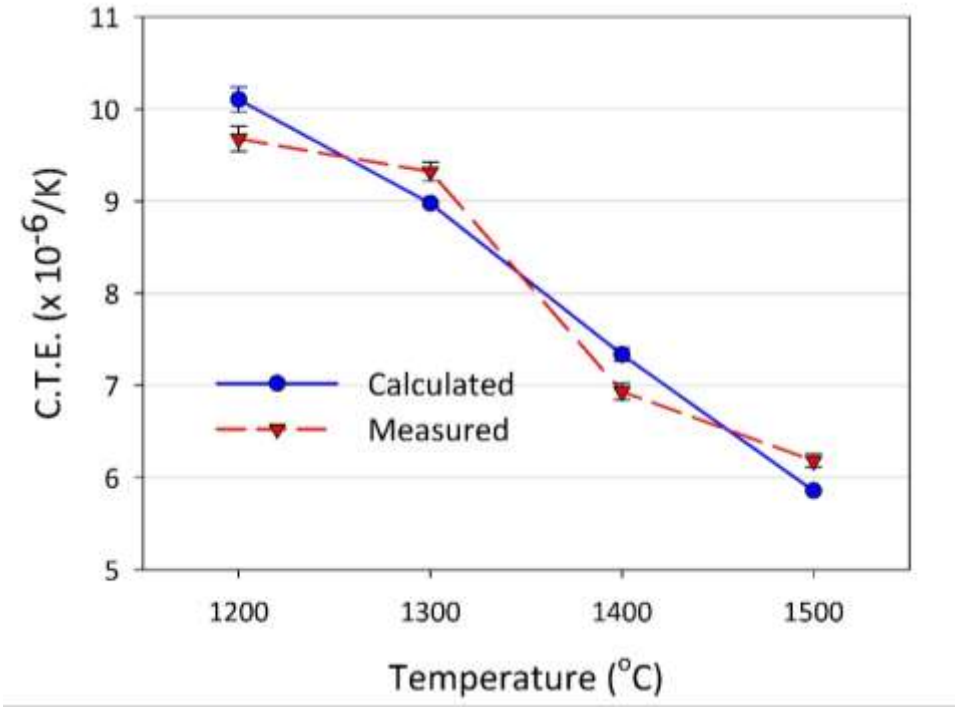

B.

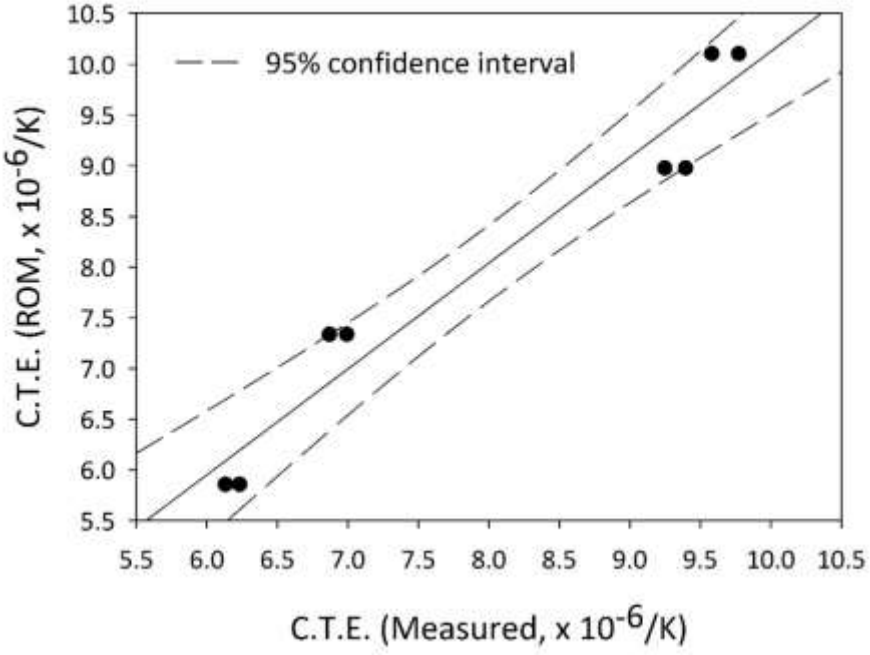

Figure 18. Measured and calculated C.T.E. values for the porcelain body fired at different temperatures (A). The trend of calculated C.T.E. values are similar to those measured (B).

Using the density and C.T.E. values, the mineralogy of the porcelain body can be predicted by plotting the properties on the volumetric ternary grid (Figure 19). The intersection between density (solid blue line) and C.T.E. (dash pink line) is the predicted mineralogy under volume basis.

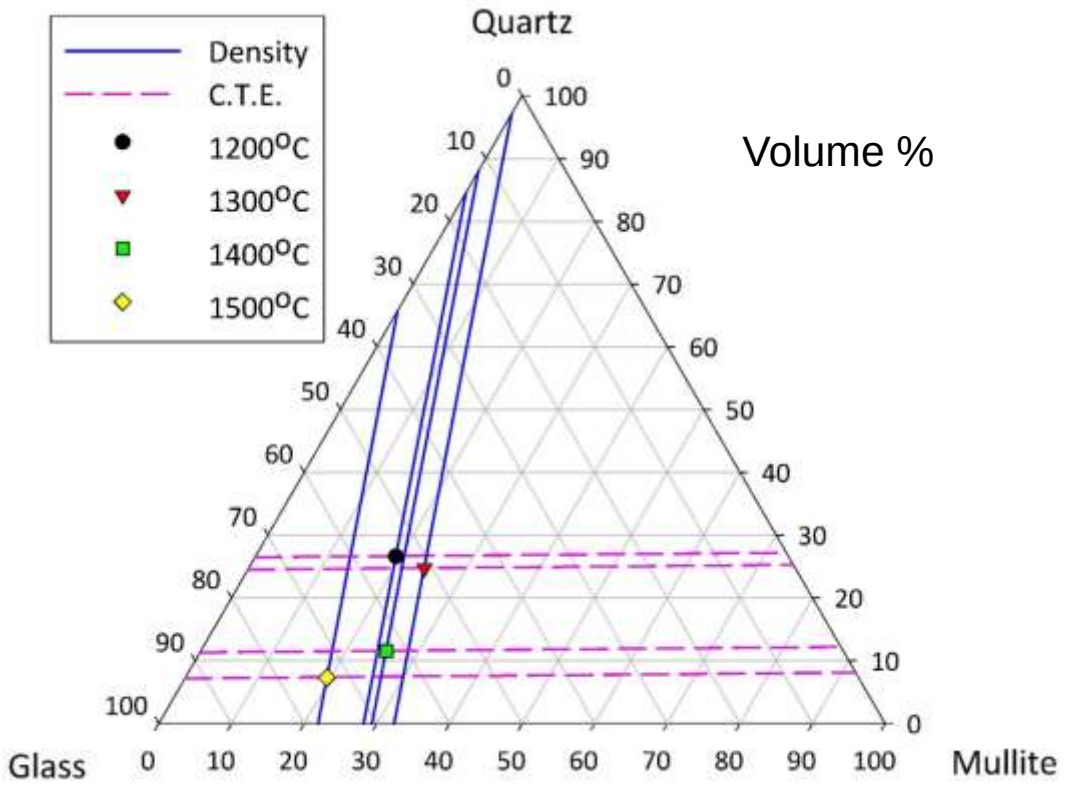

Figure 19. Intersections between density and C.T.E. properties obtained from different samples are their predicted mineralogy under volume basis.

The predicted mineralogy under volume fraction can also be translated to commonly used mass fraction basis by incorporating the density of each phase. The mineralogy obtained by QXRD and the ROM approach under mass fraction basis is plotted on the ternary diagram (Figure 20A). The results predicted via density and C.T.E. measurement are very close to the mineralogy analyzed from conventional QXRD method. A correlation coefficient (r^2) of 0.980 (Figure 20B) shows porcelain is an ideal material for this ROM approach.

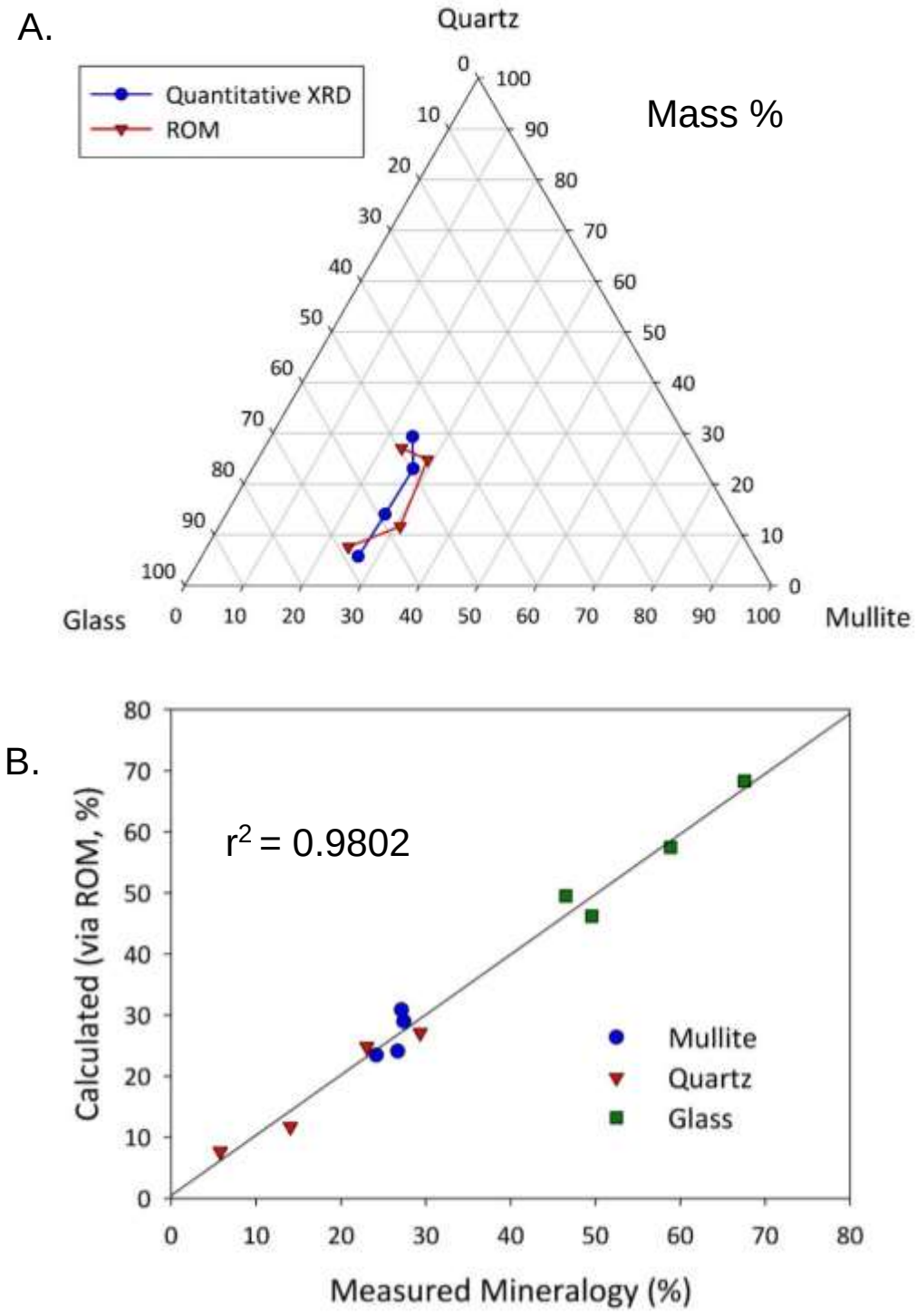

Figure 20. The predicted mineralogy for porcelain body shows good correlation compared to QXRD mineralogy (A) with an overall correlation coefficient r^2 = 0.9802 (B).

B. Mullite

Three different routes were used in mullite synthesis: kaolinitic clay with alumina (AE), silica with alumina (AS), and colloidal silica with alumina (AC). However, under the firing temperature range 1200^{o}C-1500^{o}C, neither the AS nor AC approach form significant mullite (Figure 21).[23] In the following analysis, only the mullite formation via clay and alumina will be discussed.

In mullitisation, the primary phases are composed of mullite, unreacted corundum, and glass. The impurities in the clay react to form a glass phase that is proposed to match the composition and properties (density = 2.39 g/cm^3 and C.T.E. = 4.9 x 10^{-6}/K) in porcelain body. The density and C.T.E. properties for this system are plotted on a ternary diagram (Figure 22). The properties in the mullite system also do not have the same magnitude and it follows that corundum (3.97g/cm^3) > mullite (3.17g/cm^3) > glass (2.39g/cm^3) for density and corundum (8.0 x10^{-6}/K) > glass (4.9 x10^{-6}/K) > mullite (4.7 x10^{-6}/K) for C.T.E. Compared to the porcelain system, the C.T.E. difference of each phase in the mullite system is smaller, but the difference in density values is larger.

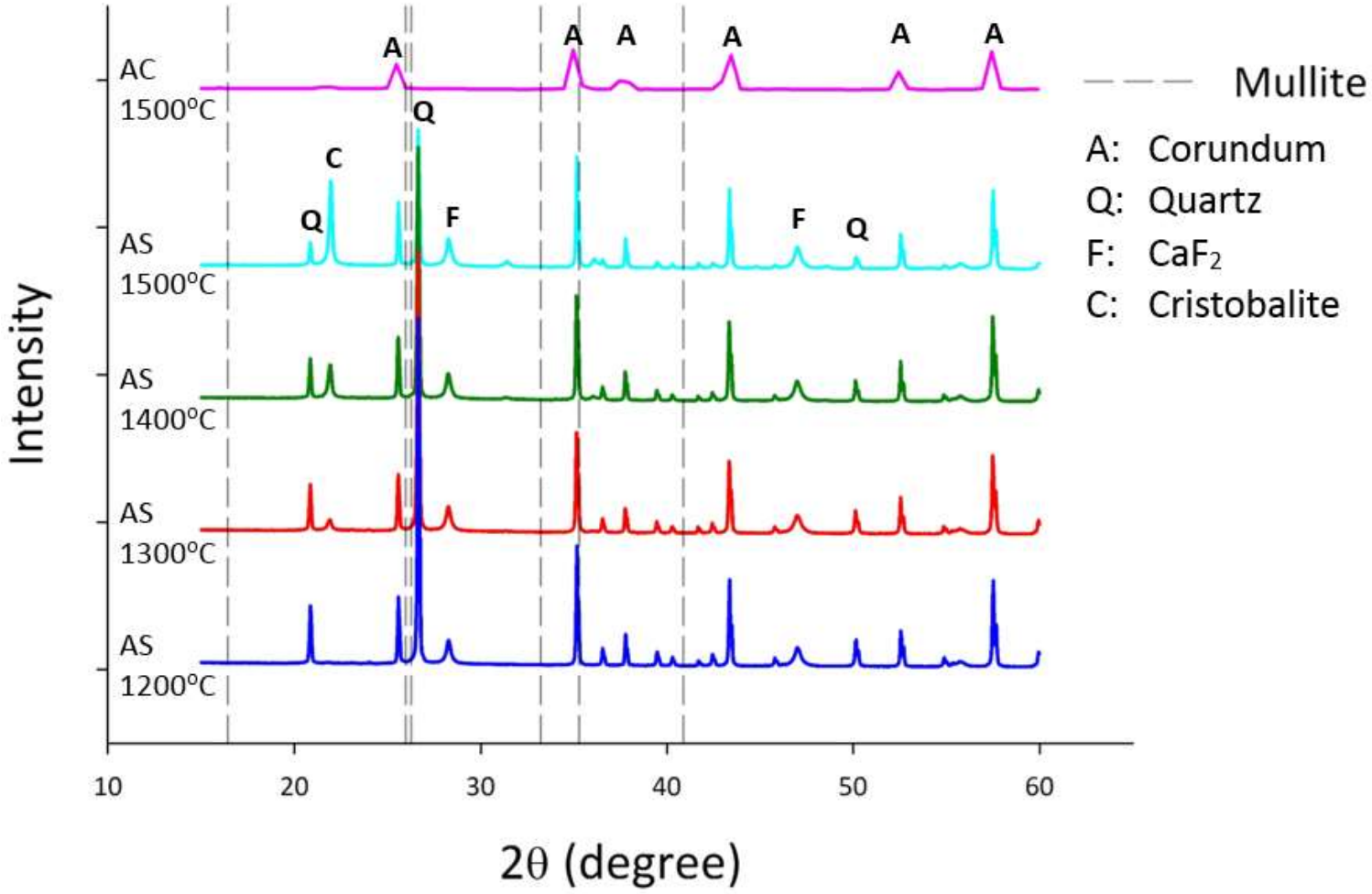

Figure 21. Mullite phase cannot be found in the XRD pattern under the synthesis temperatures for AC and AS routes.

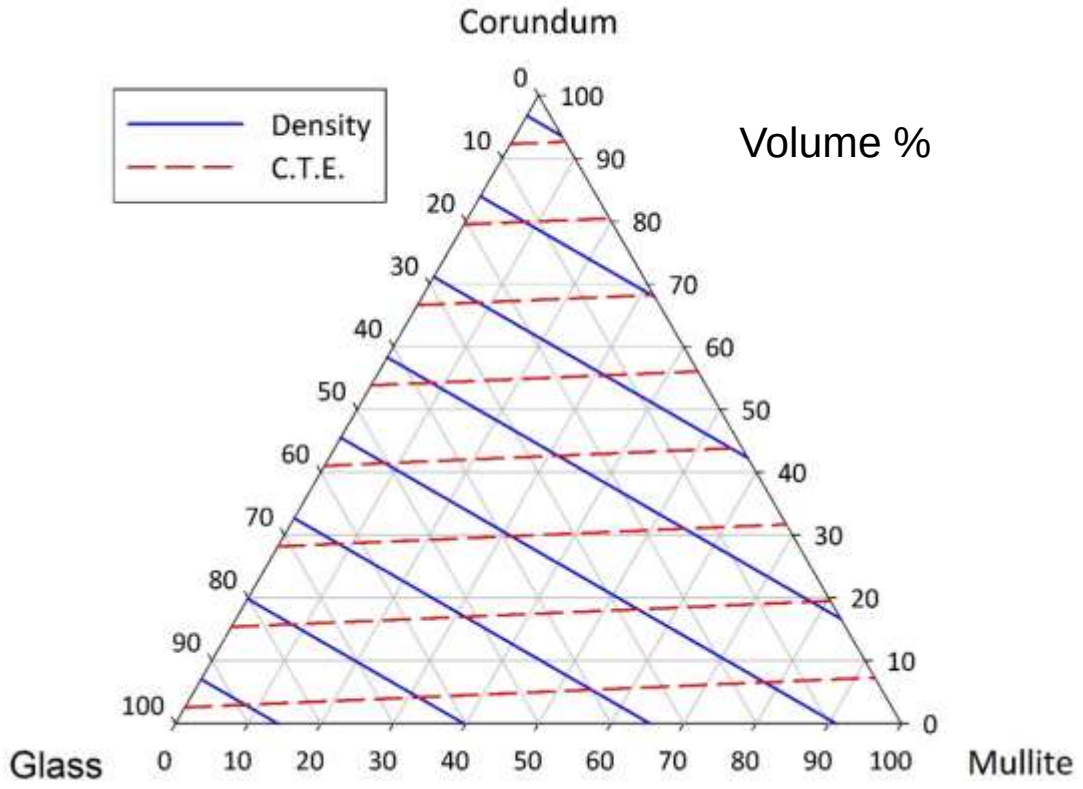

Figure 22. Volumetric grid plot of density and C.T.E. for a mixture of mullite, glass and alumina.

The QXRD mineralogy for mullite samples under temperature range 1200^{o}C-1500^{o}C is presented in Figure 23. The mullite phase exists at 1200^{o}C as primary mullite, but increases slowly before 1400^{o}C. After 1400^{o}C, unreacted corundum and silica start the secondary mullite formation. The amount of glass phase is balance by the fraction difference of mullite and corundum phases.

A.

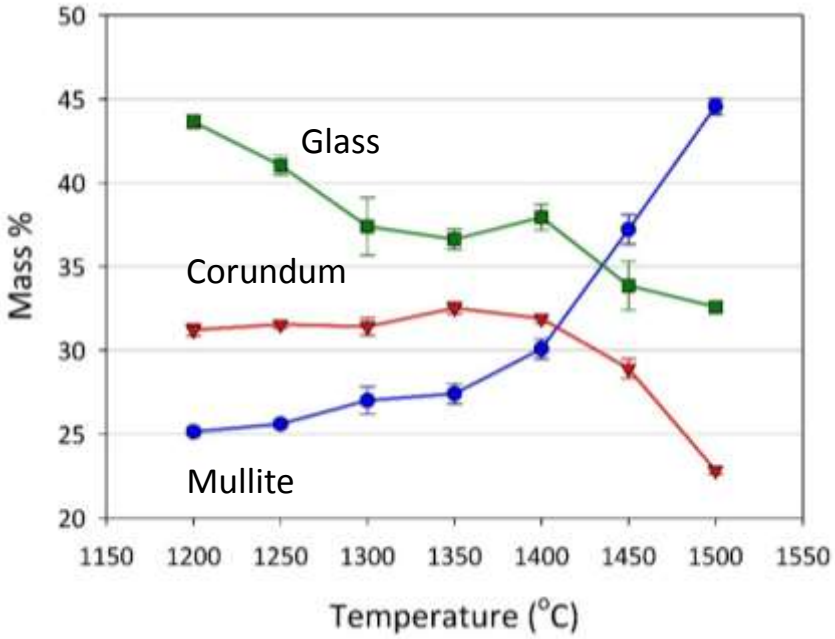

B.

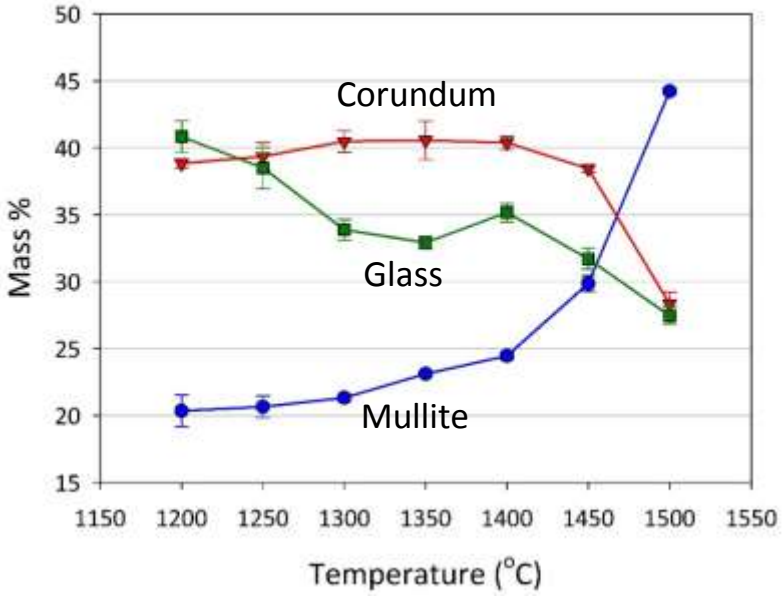

Figure 23. The QXRD mineralogy of AE42(A), AE52 (B), and AE62(C). The primary mullite formation starts from 1200°C. Secondary mullite formed by unreacted corundum and glass starts from 1400°C. The glass phase is the fraction balance by other two phases.

C.

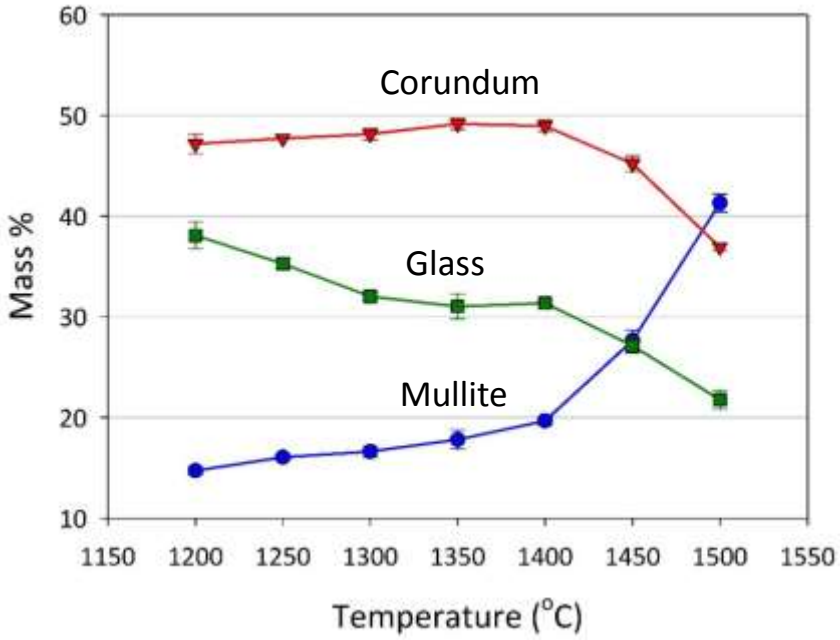

Figure 23 (cont.). The QXRD mineralogy AE42(A), AE52 (B), and AE62(C). The primary mullite formation starts from 1200°C. Secondary mullite formed by unreacted corundum and glass starts from 1400°C. The glass phase is the fraction balance by other two phases.

The measured density and C.T.E. values are plotted in Figure 24 and 25 compared with the properties calculated through ROM equations by the composition of each sample. Under the temperature range 1250°C-1350°C, an unexpected C.T.E. result shows that the measurement values are significantly higher than ROM calculation. The calculated density values are also higher than measured density at 1300°C and 1350°C. The predicted mineralogy under temperature range 1250°C-1350°C cannot be found (no intersection) from ROM calculation (Figure 26).

A.

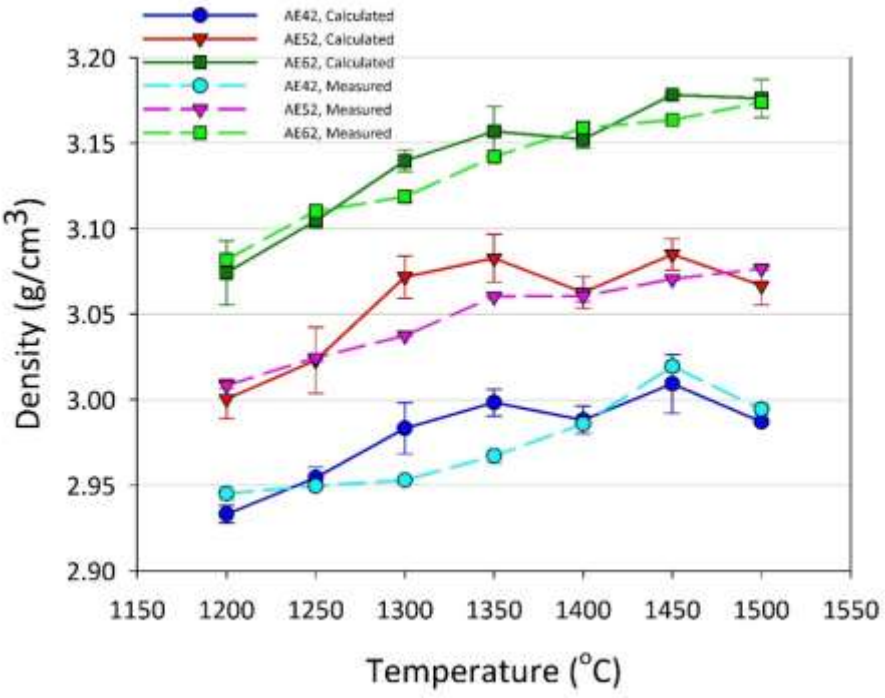

B.

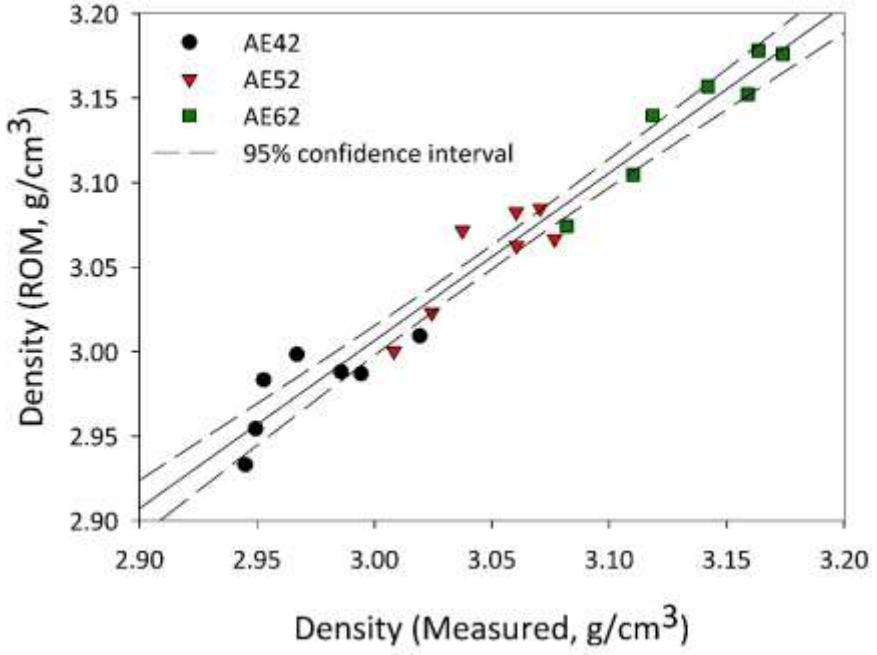

Figure 24. Measured (dashed) and calculated (solid) density values (A) with the comparison (B). The calculated density values are slightly higher than measurements at 1300°C and 1350°C.

A.

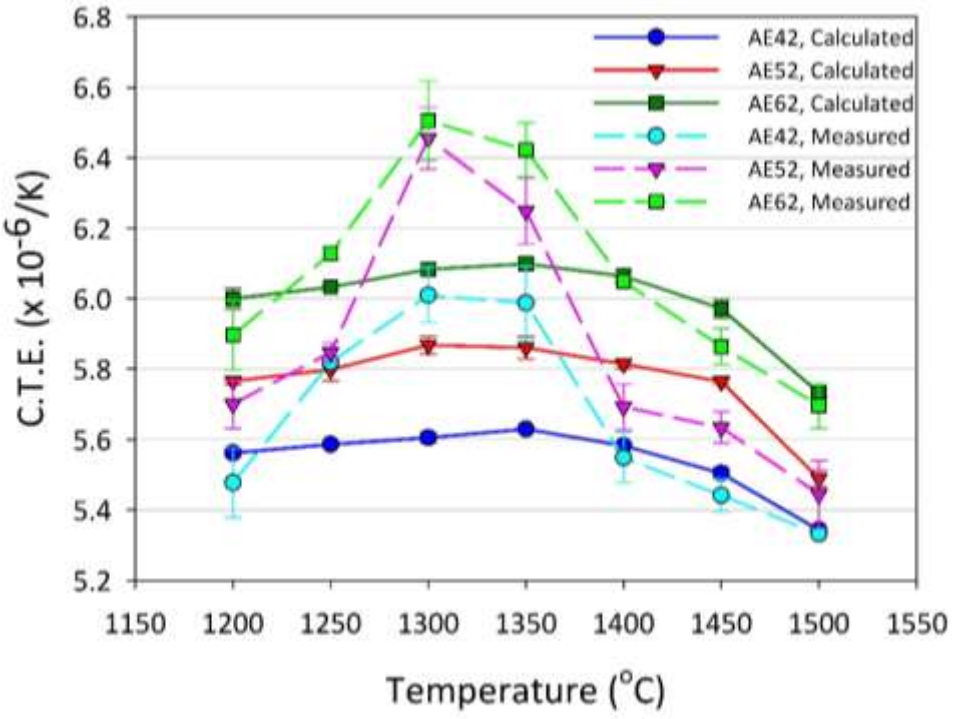

B.

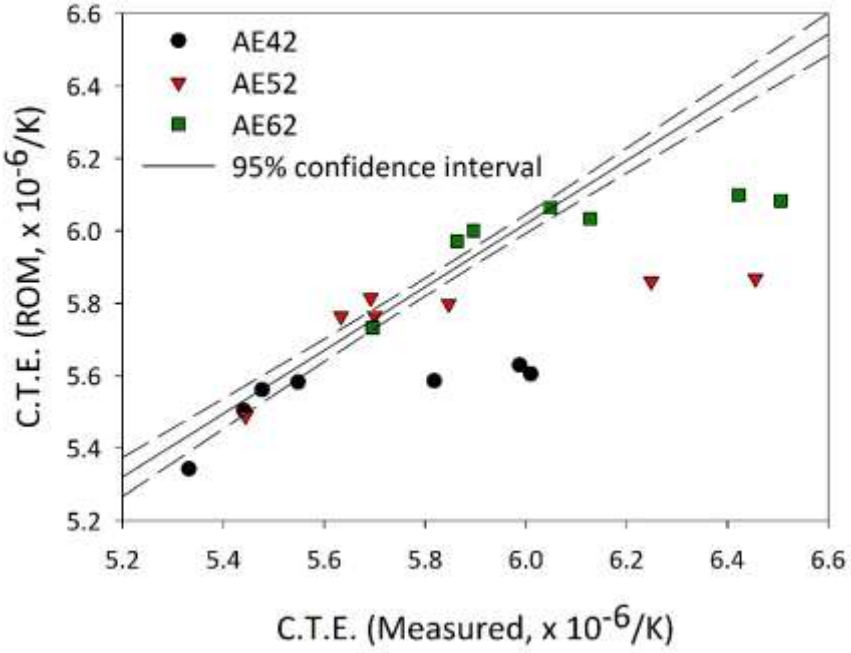

Figure 25. Measured (dashed) and calculated (solid) C.T.E. values (A) with the comparison (B). Under temperature range 1250°C-1350°C, the calculate C.T.E. values are significantly lower than the measurements.

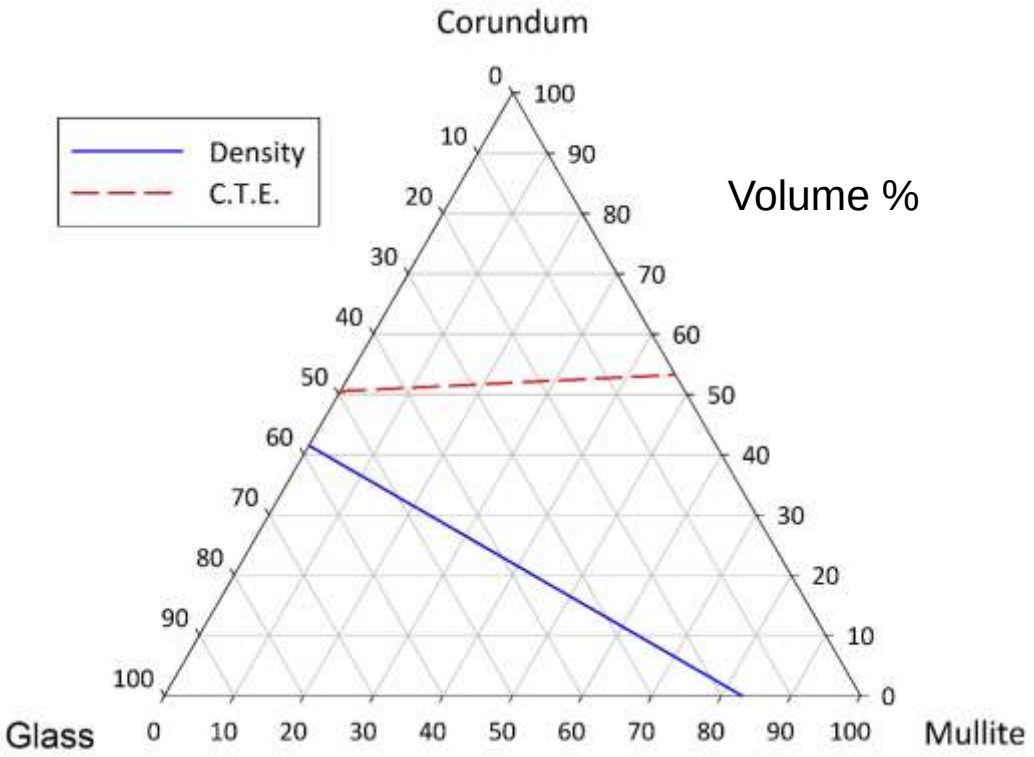

Figure 26. The predicted mineralogy cannot be found in ternary diagram. Take sample AE52 at 1300^{o}C as an example.

To figure out the problem of mullite samples under this temperature range, the XRD pattern (Figure 27) is examined to find any impurities contained in mullite samples. The small amount of cristobalite is found in all three starting compositions under this temperature range, which also exists in previous works.[24,29] The cristobalite phase exists from 1250^{o}C and disappear at 1400^{o}C (Figure 28) due to the reaction with corundum. The density value of cristobalite (2.32 g/cm^{3}) is slightly lower the glass phase (2.39 g/cm^{3}) so there is limited error generated. Compared to other phases, the high C.T.E. value (14.5 x10^{-6}/K) of cristobalite, however, contributes significantly to C.T.E. value of sample. After containing this unexpected phase in ROM calculation for density and C.T.E., the offset values between measured and calculated can be corrected (Figure 29 and 30).

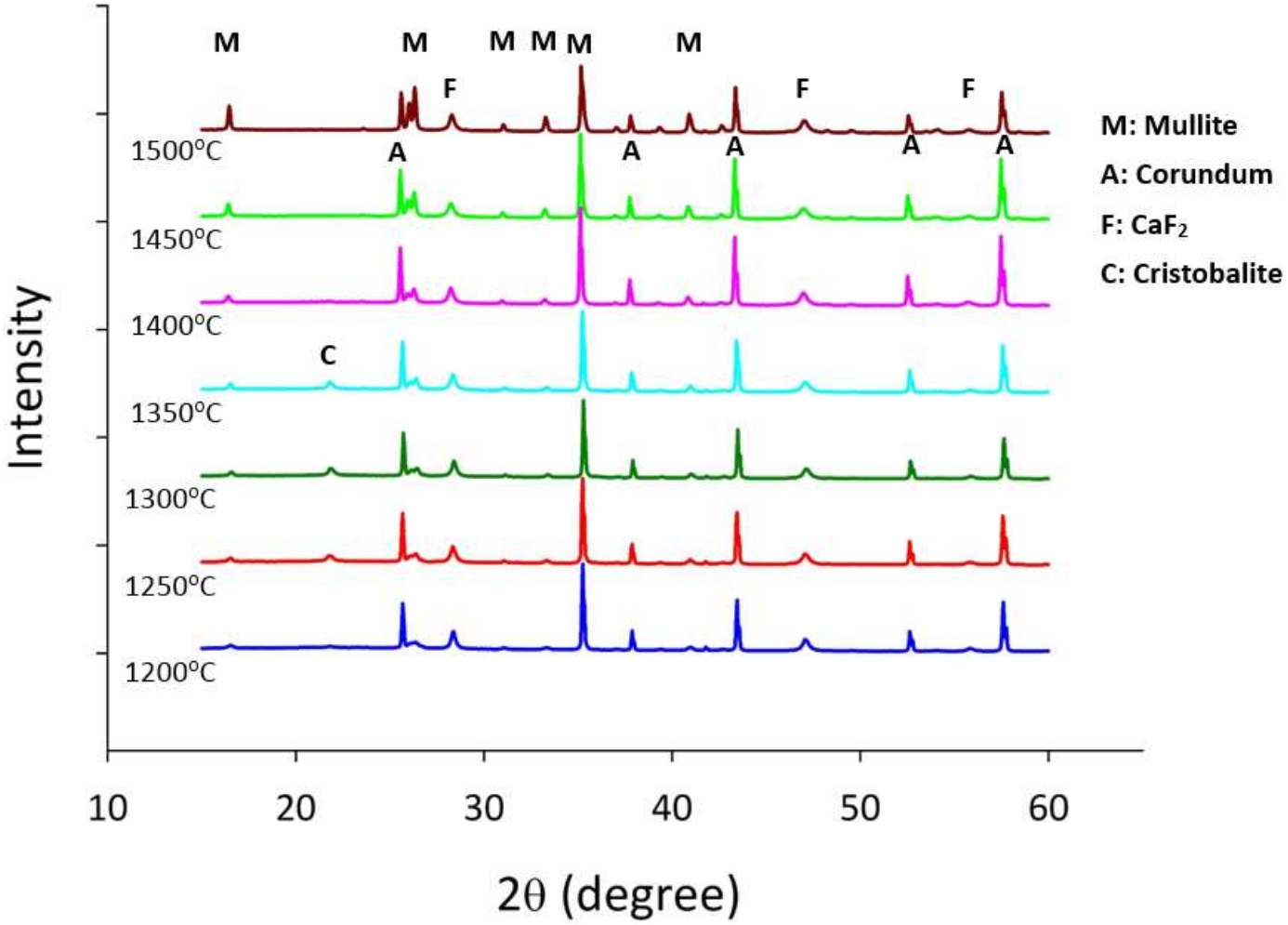

Figure 27. XRD pattern for AE62 system. Cristobalite phase exists under temperatures 1250°C-1350°C.

A.

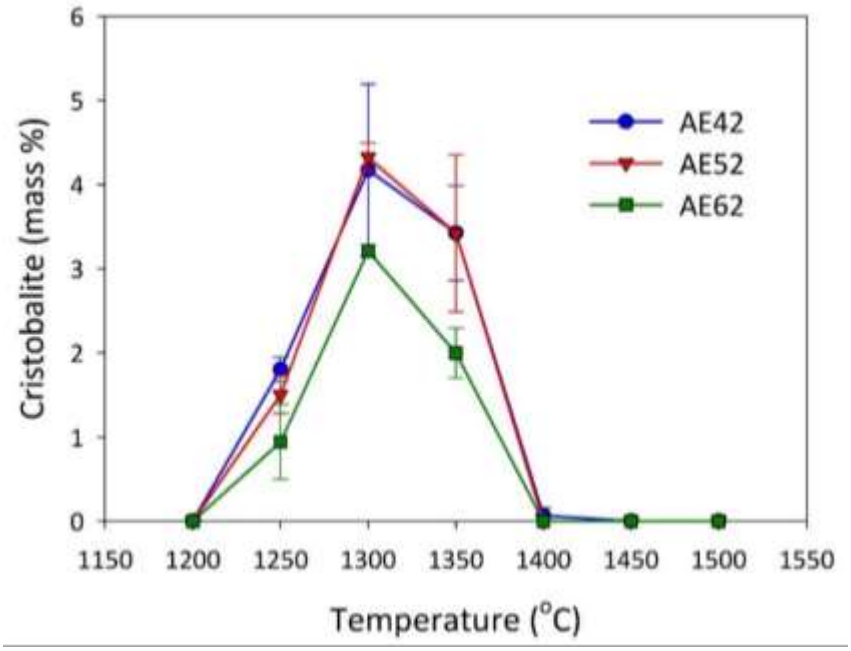

B.

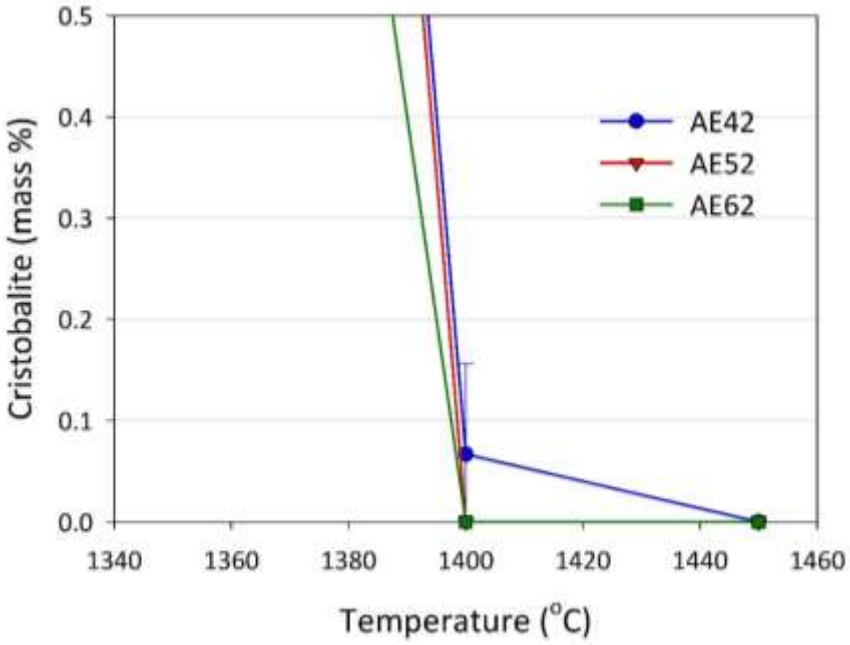

Figure 28. Cristobalite phase exists in mullite samples under temperature range 1250°C-1350°C (A). The sample AE42 at 1400°C shows a small amount of cristobalite (<0.1%) which can be ignored (B).

A.

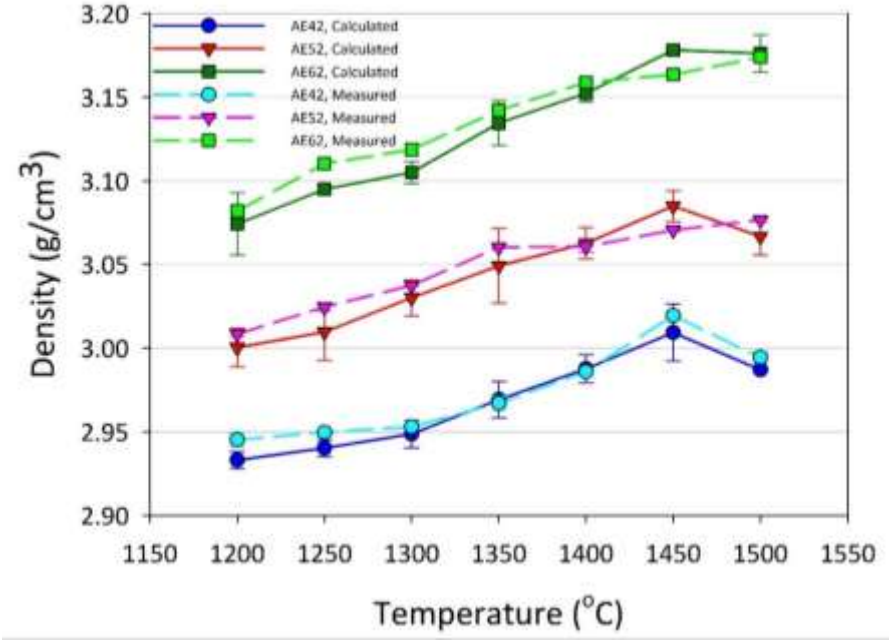

B.

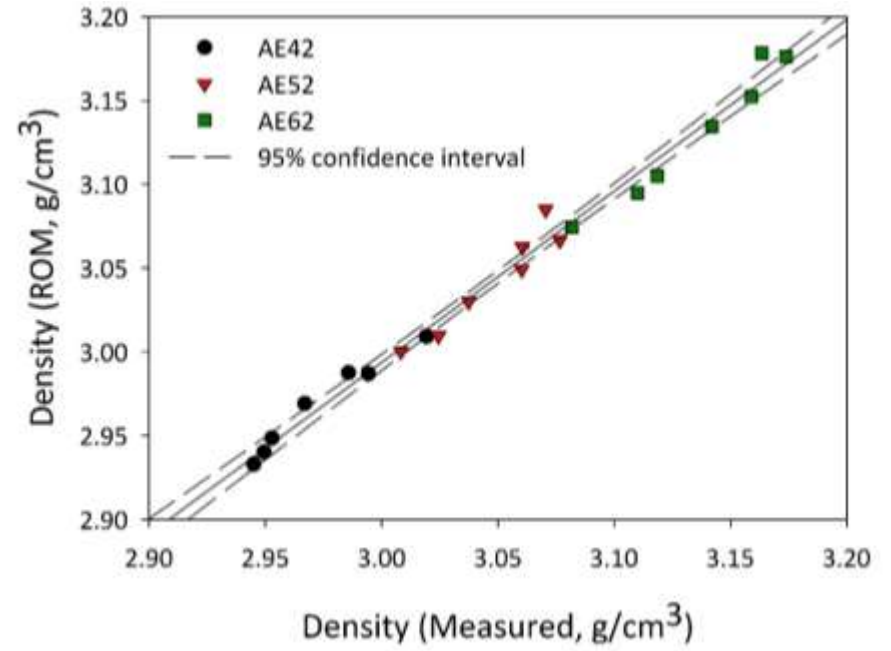

Figure 29. Measured (dashed) and calculated (solid) density values (A) with the comparison (B). After the cristobalite phase is included, the calculated density values can be corrected.

A.

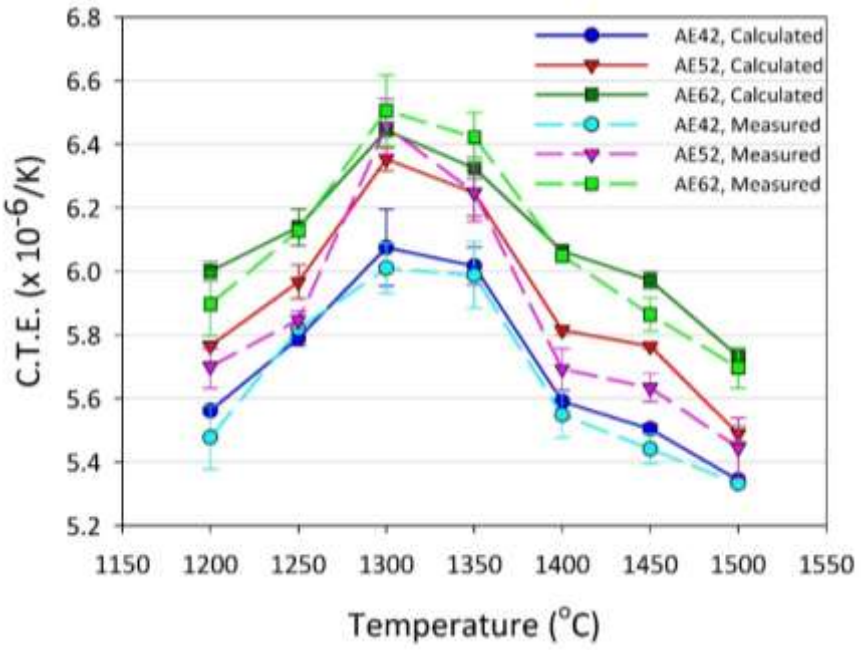

B.

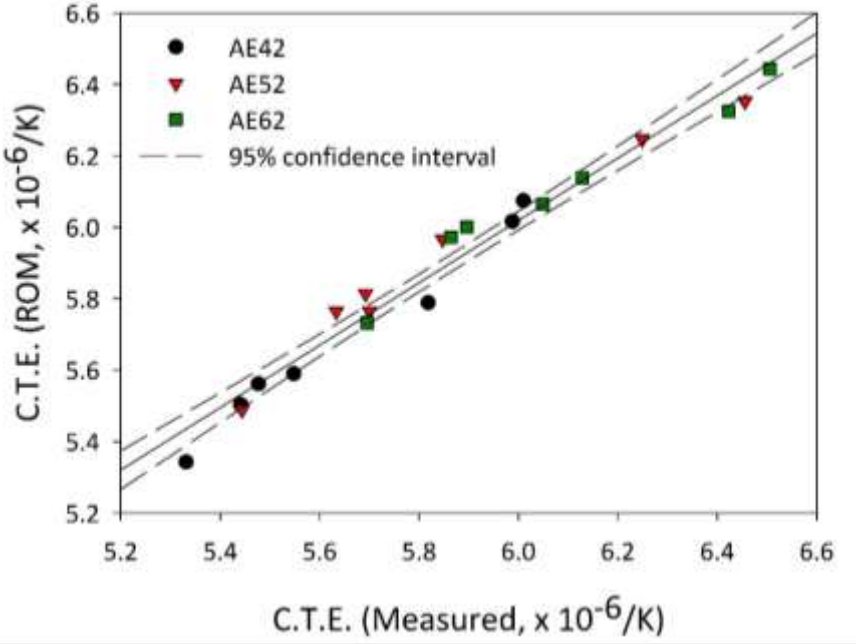

Figure 30. Measured and calculated C.T.E. values via XRD composition incorporating the presence of cristobalite (A) with the comparison (B).

Under the temperature range where cristobalite is present, the mineralogy is no longer three components but four components. As a result, the temperature range 1250^{o}C-1350^{o}C cannot be used for this approach. In conclusion, if mineralogy cannot be predicted through the ROM approach, it may be that impurity mineral phase contributes to the measured properties.

Figure 31A shows the mineralogy of QXRD and prediction in a mass-based ternary diagram, omitting the mineralogy under 1250^{o}C-1350^{o}C, whereas these samples contain cristobalite. The QXRD and predicted mineralogy for all three samples show a low correlation coefficient 0.831 (Figure 31B). The mullite level from prediction is overestimated than QXRD and corundum level is underestimated.

A.

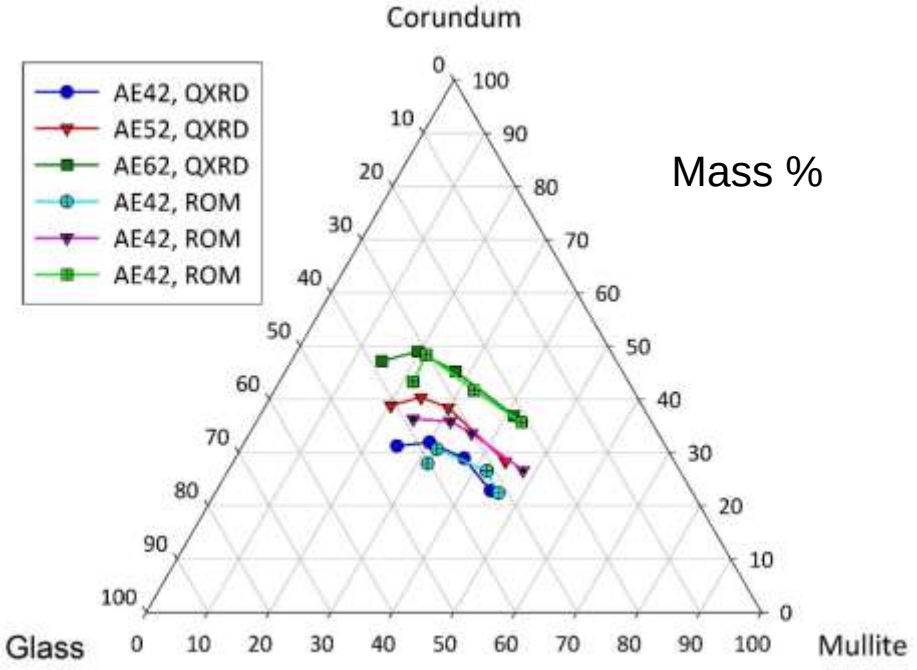

B.

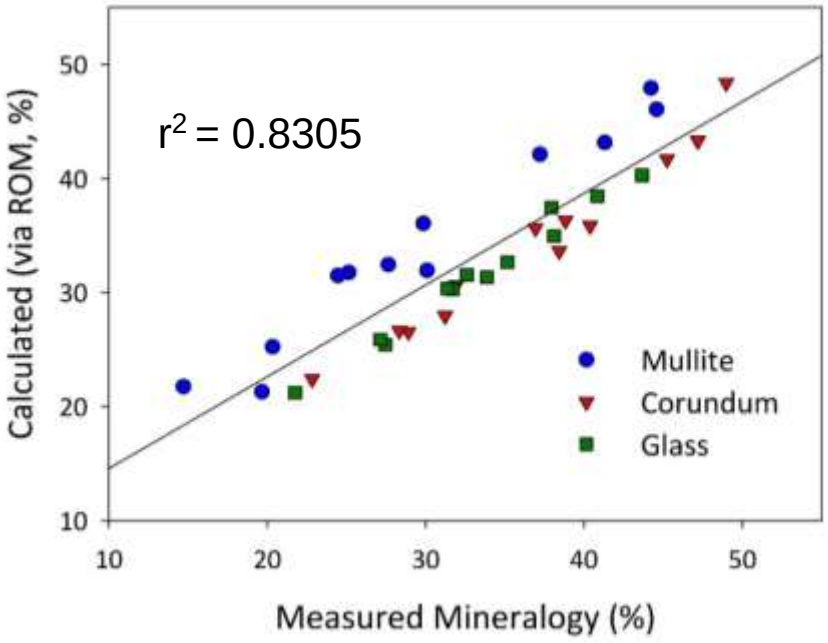

Figure 31. Measured and predicted mineralogy of the reaction of clay and alumina on a mass based ternary diagram (A) and comparison (B). Compared to measured mineralogy via QXRD, the predicted mullite level is higher and the corundum level is lower.

The difference in mineralogy can be generated via the lower measured C.T.E. values compared to calculated C.T.E. (Figure 32) due to the high C.T.E. value of corundum (8.0 $x10^{-6}$/K) compared to mullite (4.7 $x10^{-6}$/K) and glass (4.88 $x10^{-6}$/K). From previous research, the thermal expansion coefficient of the glass decreases with increasing molar percentage of silica and alumina (Figure 33).[11,30,31] The molar percentage of silica and alumina of glass phase are similar for the porcelain (94.0%) and mullite bodies (97.0%) in this study. Thus the C.T.E. value of glass phase in mullite synthesis can be corrected (4.71 $x10^{-6}$/K) and is still within the margin for error in the previous measurements. The corrected C.T.E. values match well with measurements (Figure 34). The large difference of elastic modulus among components can also be an issue but it is assumed to contribute minor affect after the C.T.E. value of glass phase is corrected. The corrected mineralogy shows a good correlation with QXRD mineralogy with r^2 = 0.9694 (Figure 35).

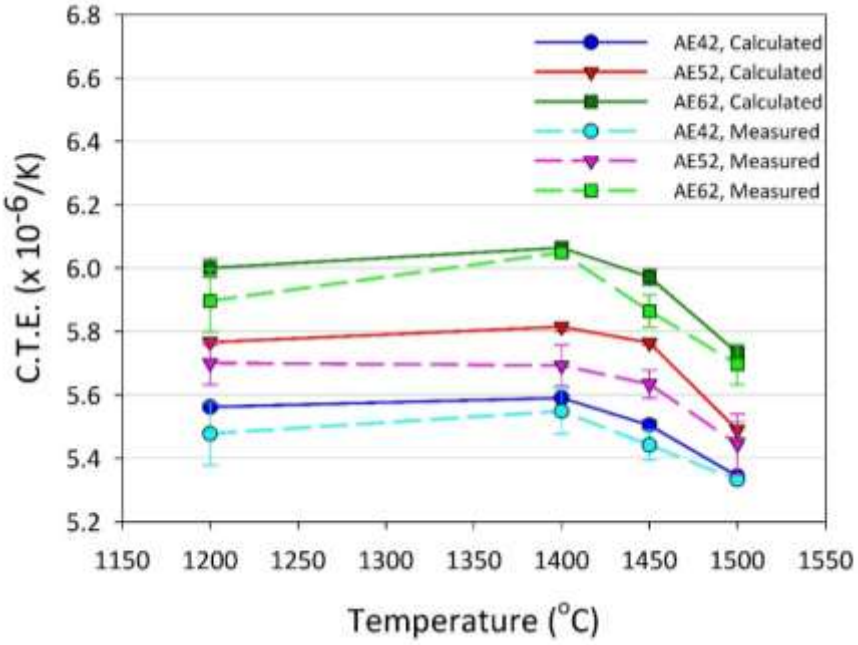

Figure 32. Measured C.T.E. values are slightly lower than calculated C.T.E values.

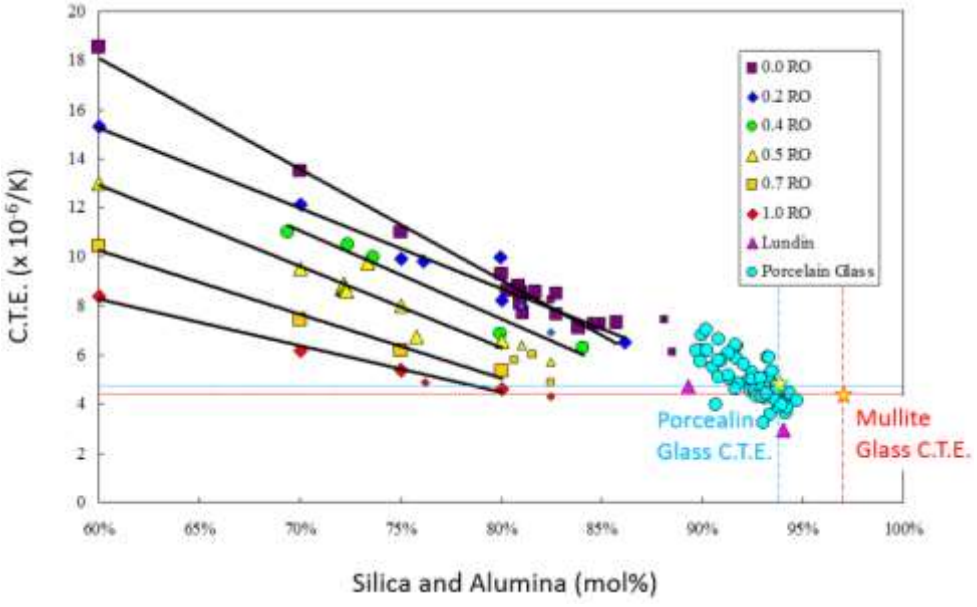

Figure 33. The C.T.E. values for the porcelain glass and mullite glass agree with the trends of previous work.[11,30,31]

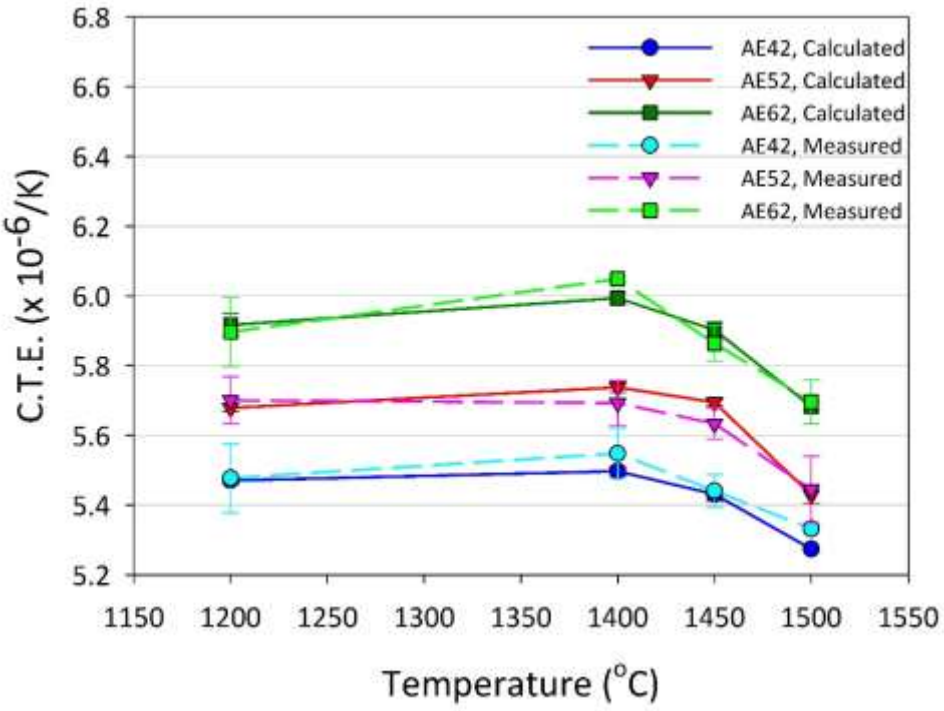

Figure 34. After the C.T.E. value of glass is corrected, the measured and calculated C.T.E. match well.

A.

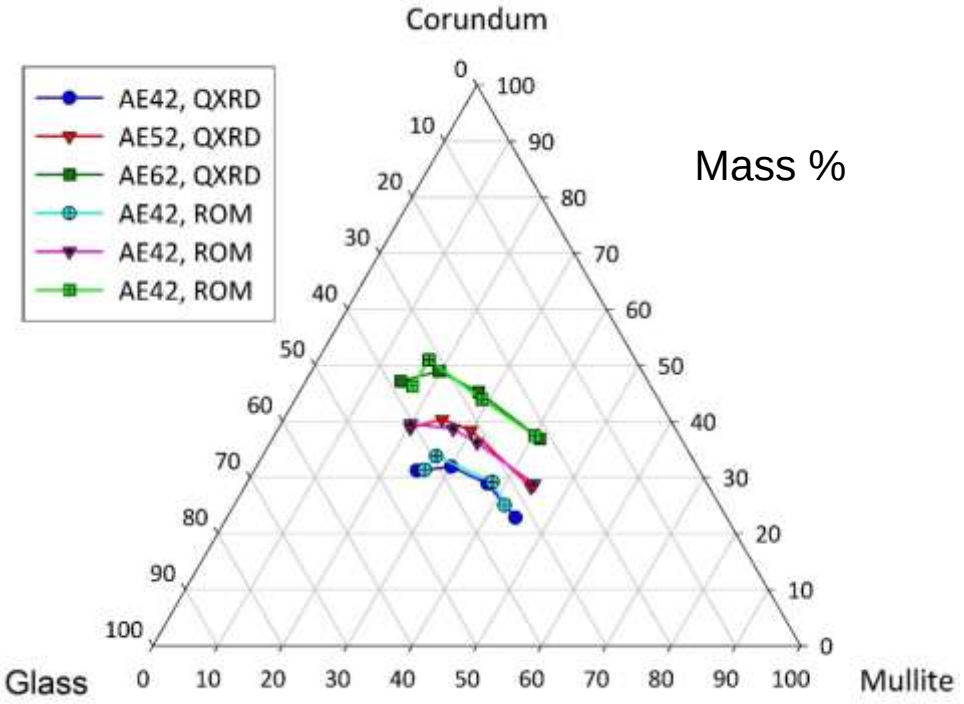

B.

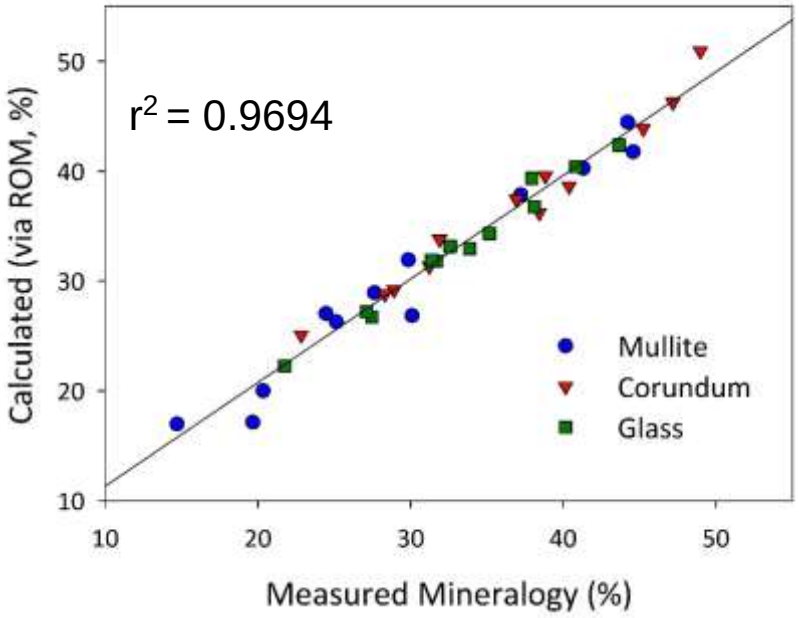

Figure 35. Measured and predicted mineralogy after the correction of mullite glass.

C. Spinel

Magnesium aluminate spinel ($MgAl_2O_4$) can be synthesized via the reaction of alumina and magnesium oxide. The final mineralogy in this experiment is composed of three components: spinel, unreacted alumina, and magnesium oxide. The nature of properties fulfilling the requirements for the ROM approach are plotted in Figure 36. The density values of magnesium oxide (3.58 g/cm^3) and spinel (3.60 g/cm^3) are similar, therefore the density of the spinel sample is dominated by the alumina phase (3.97 g/cm^3).

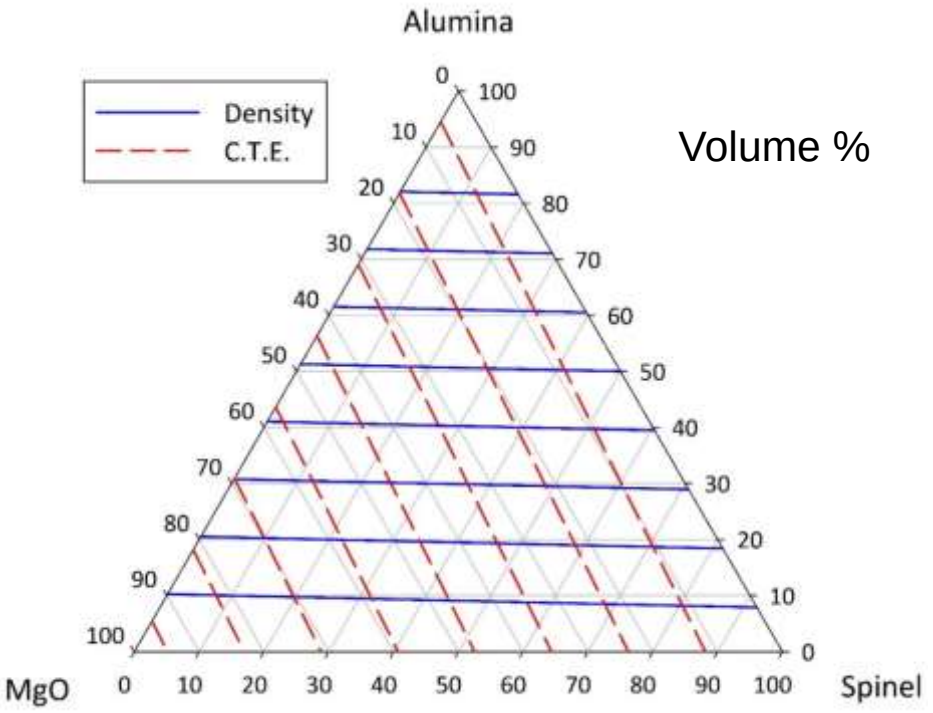

Figure 36. Volumetric ternary diagram of spinel system with density and C.T.E. grids.

The mineralogy of spinel synthesis via alumina and magnesium oxide reaction can be analyzed from QXRD (Figure 37). At 1600°C, the synthesis reaction is almost completed and the main phases in the sample are spinel and excessive magnesium oxide.

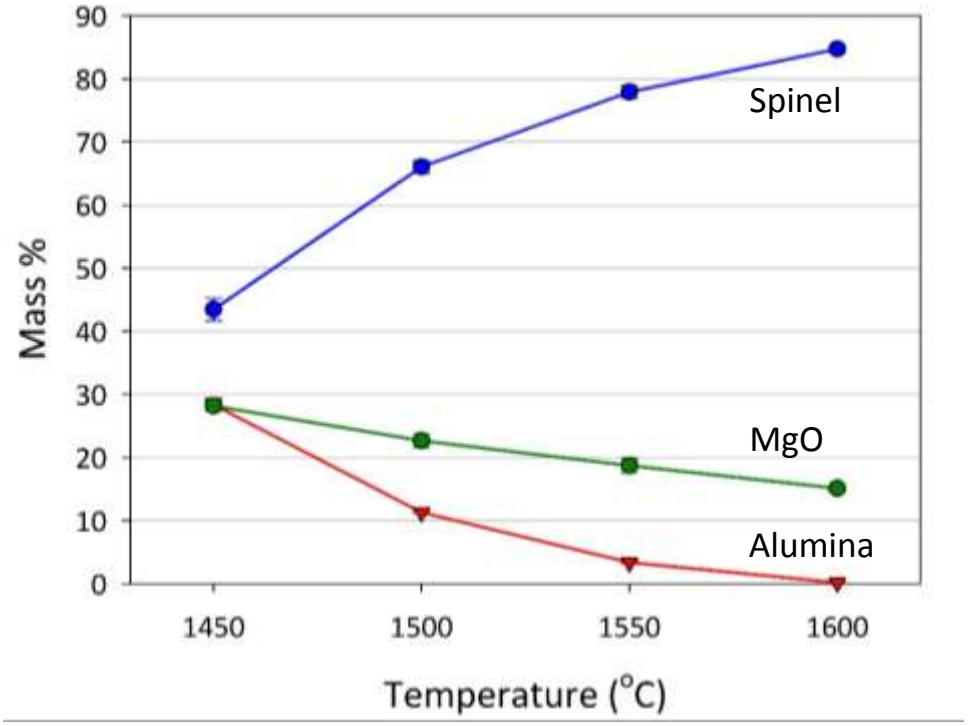

Figure 37. The mineralogy of spinel samples analyzed by QXRD. Compositions of alumina and magnesium oxide decrease with an increase of temperature to synthesize spinel. At 1600°C, the spinel formation is almost done with excessive magnesium oxide left over. The MgO phase is the fraction balance by other two phases.

Figure 38 and 39 are plots of measured density and C.T.E. values as a function of temperature. The density difference in spinel system is not large and is dominated by alumina component. As a result, the densities fall in a small

range and decrease with the alumina component. The offset of C.T.E. values at 1450^{o}C and 1500^{o}C can be due to the difference of elastic modulus. The elastic modulus values of spinel (250.7 GPa) and magnesium oxide (230.28 GPa) are similar; however, the elastic modulus of alumina is higher (376.9 GPa).[14] At temperature 1450^{o}C and 1500^{o}C, the measured C.T.E. values is offset from the calculation due to the interference of elastic modulus. After 1500^{o}C, the amount of alumina is less than 10% and the difference between measured and calculated C.T.E. is smaller. The mechanism that how the difference of elastic modulus could shift the C.T.E. value has not been evaluated.

The mineralogy of the spinel sample predicted by this ROM approach is plotted in Figure 40 with correlation coefficient 0.927.

A.

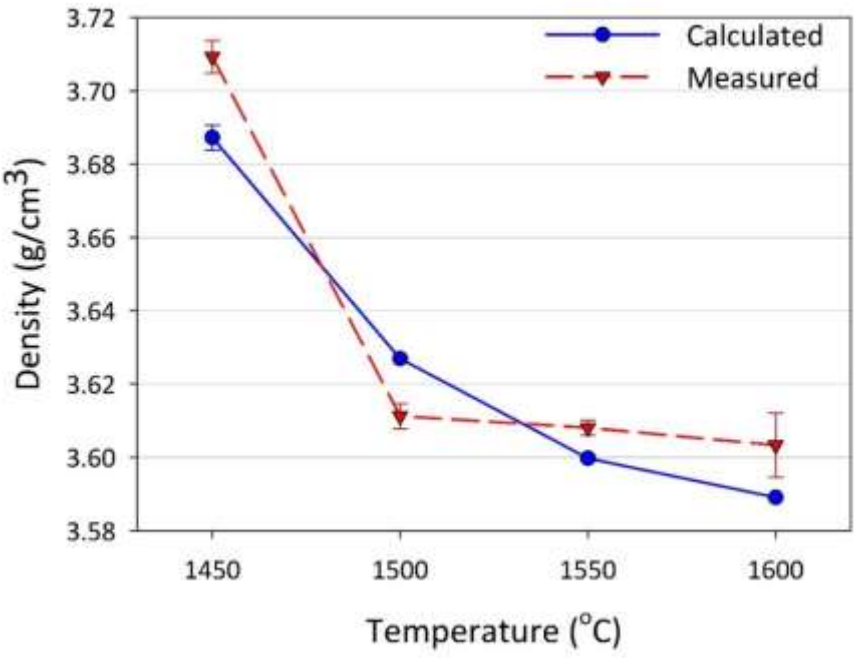

B.

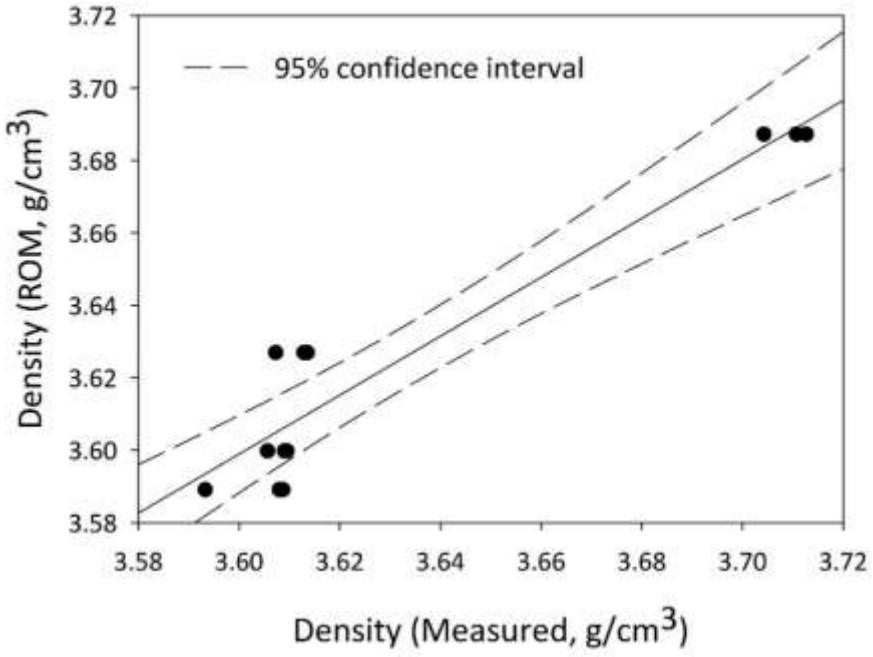

Figure 38. Measured and calculated density values for a spinel body fired at different temperatures (A) and regression relationship (B).

A.

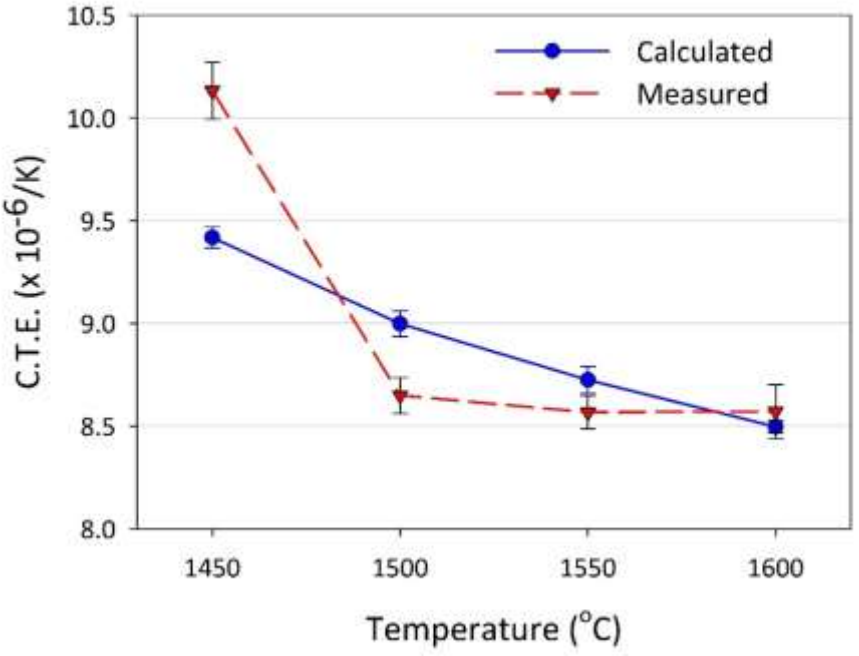

B.

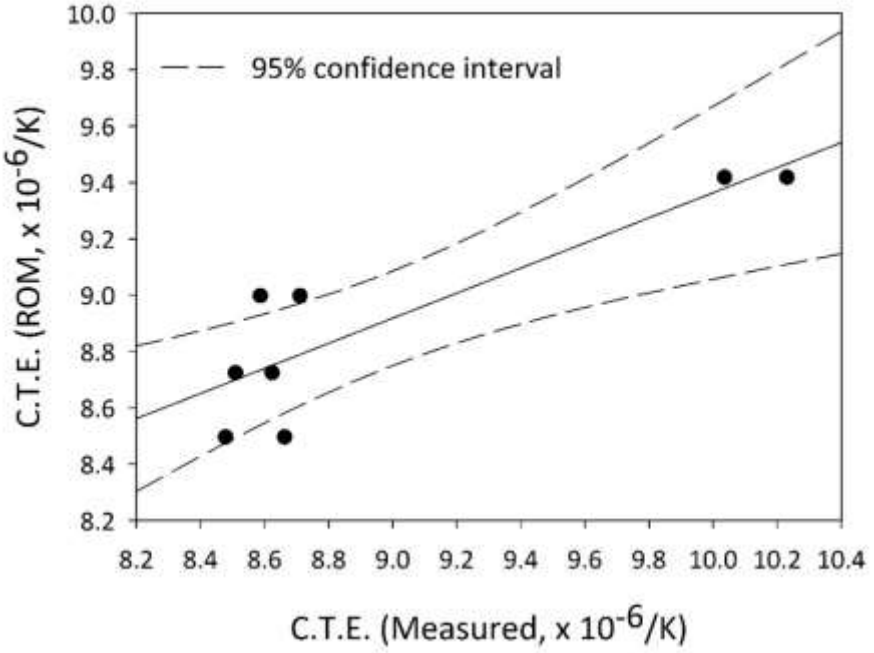

Figure 39. Measured and calculated C.T.E. values for a spinel body fired at different temperatures (A) with the comparison (B). The measured C.T.E. values at 1450°C and 1500°C are slightly offset from calculated values.

A.

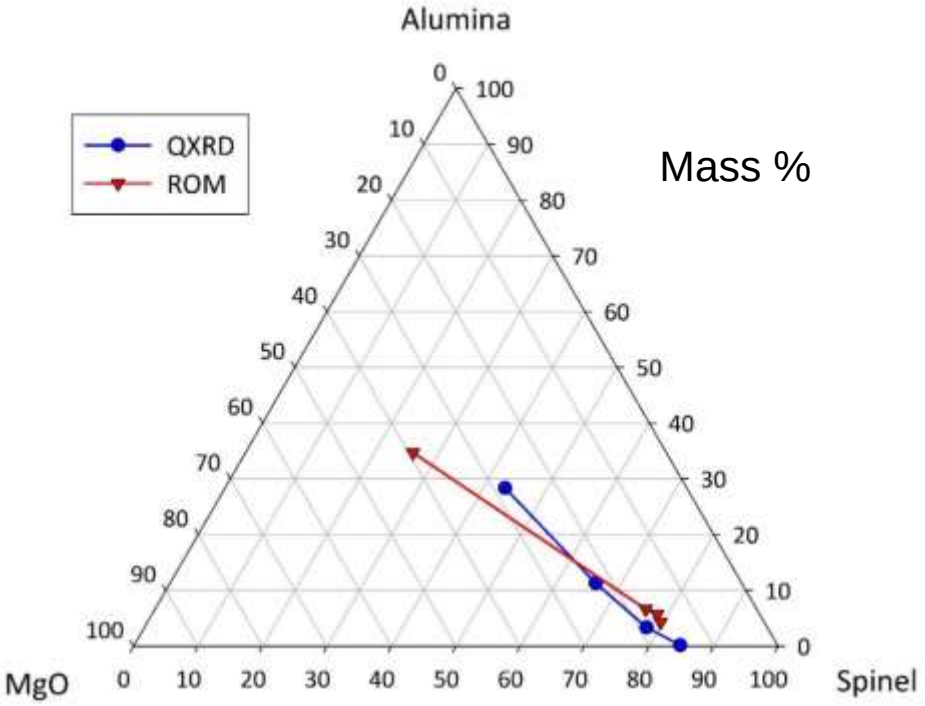

B.

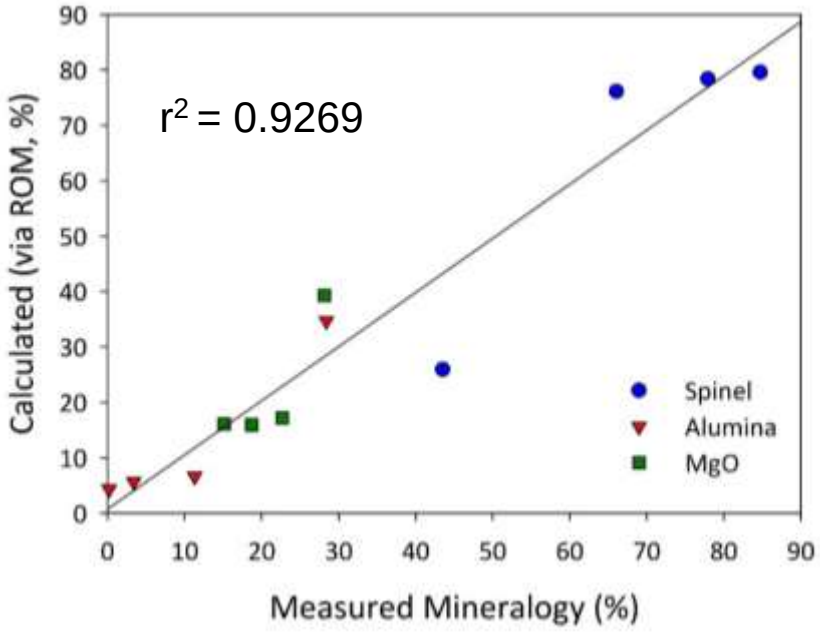

Figure 40. Measured and predicted mineralogy for spinel shows a good correlation with r^2 = 0.9269. The predicted mineralogy is calculated by measured density and C.T.E. values.

The spinel system is a promising experiment for this approach because the mineralogy also can be obtained from its chemistry constraint with only one property measured. The formation on magnesium aluminate spinel can be synthesized by simple chemistry reaction of magnesium oxide with calcined alumina (Equation 18). This reaction provides a chemistry constraint since it is not likely that a liquid or glass phase would be formed during sintering. The chemistry constraint can also be plotted linearly on the ternary diagram (Figure 41). The chemistry constraint is controlled by the starting raw materials. The stoichiometric mixing of alumina and magnesium oxide can form 100% spinel after reaction completed. With higher or lower Al_2O_3/MgO ratio as starting chemistry, the final products can be spinel with excessive alumina or magnesium oxide. Therefore, it may be possible to predict the mineralogy from C.T.E. (or density) measurements in conjunction with the chemistry, thus eliminating the need for additional property measurements. It is preferred to predicted mineralogy from density than C.T.E. with chemistry because the grids formed by the latter group are similar, which disobey the second requirement in ROM approach.

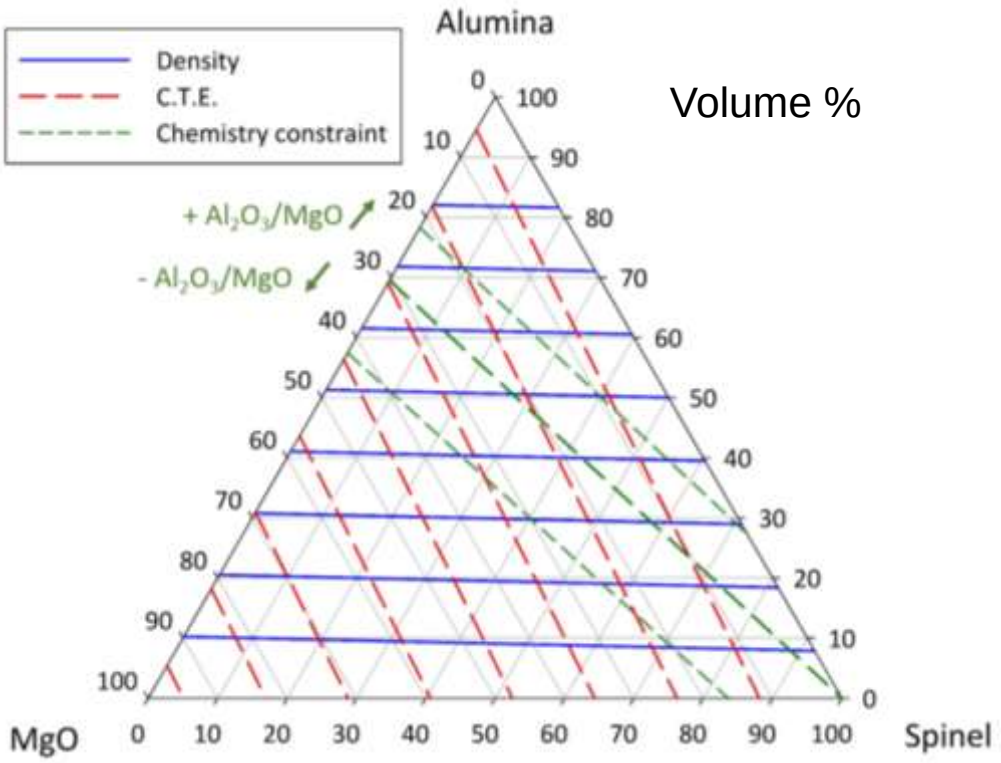

Figure 41. Chemistry constraint can be plotted on the ternary diagram. The starting chemistry can be change via different ratio of raw materials. With one property (density or C.T.E.) measured, the mineralogy can be obtained.

Using measured density values with starting chemistry (40 wt.% magnesium oxide- 60 wt.% alumina), the mineralogy can be predicted on the ternary grid diagram (Figure 42A) compared to the QXRD analysis under mass fraction basis. The predicted mineralogy shows a good result with correlation coefficient of 0.968 (Figure 42B).

A.

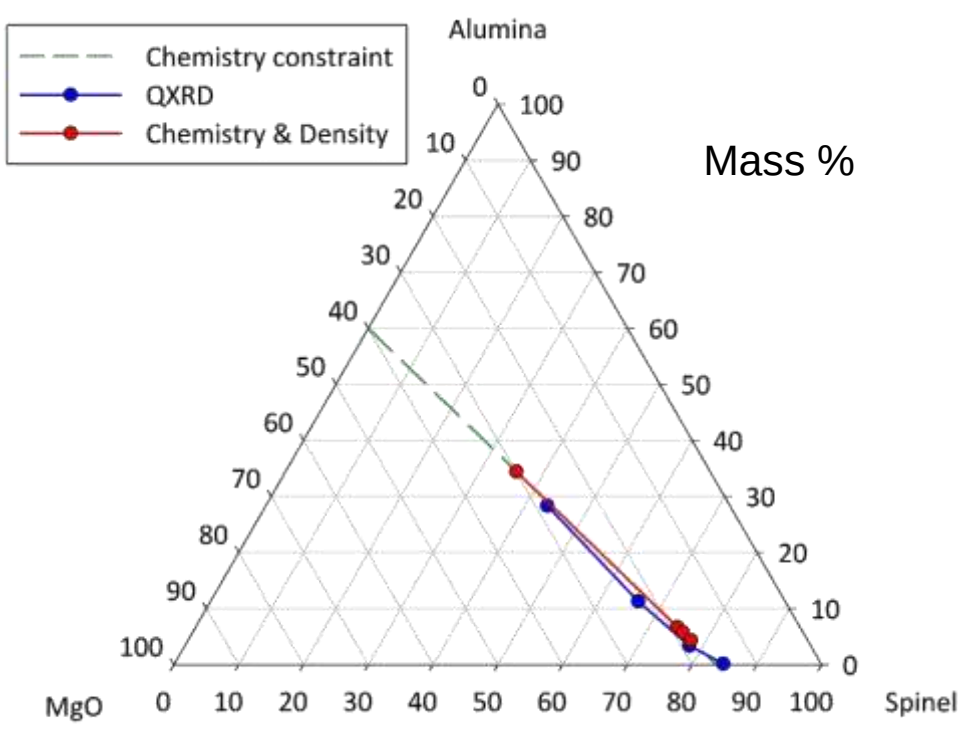

B.

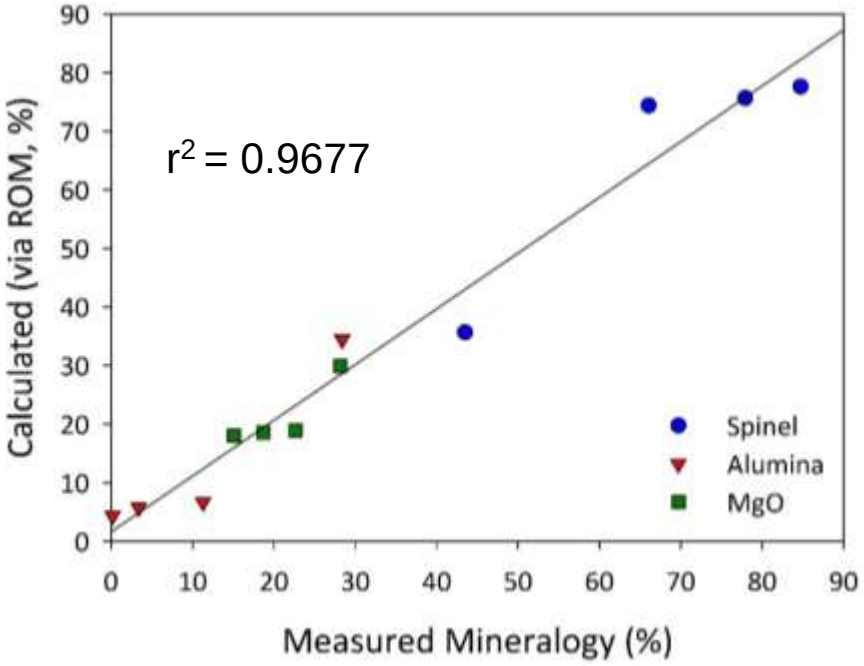

Figure 42. The mineralogy predicted from the starting chemistry and measured density.

With chemistry constraint, the C.T.E. values also can be used as a property to predict mineralogy, which is shown on Figure 43. The difference is large between predicted and QXRD mineralogy, with correlation coefficient 0.8187. The first reason is because the C.T.E. values is affected by the large difference of elastic modulus between phases. The other reason of low accuracy is due to the grids formed by chemistry constraint and C.T.E. increasing consistently in ternary diagram (Figure 44), which is the second restriction for the ROM approach. The accuracy of this ROM approach decreases significantly under this circumstance because a slight difference in measured C.T.E. values can remarkably change the predicted mineralogy. As a result, the mineralogy can be predicted using the chemistry and C.T.E. measurements in spinel synthesis.

A.

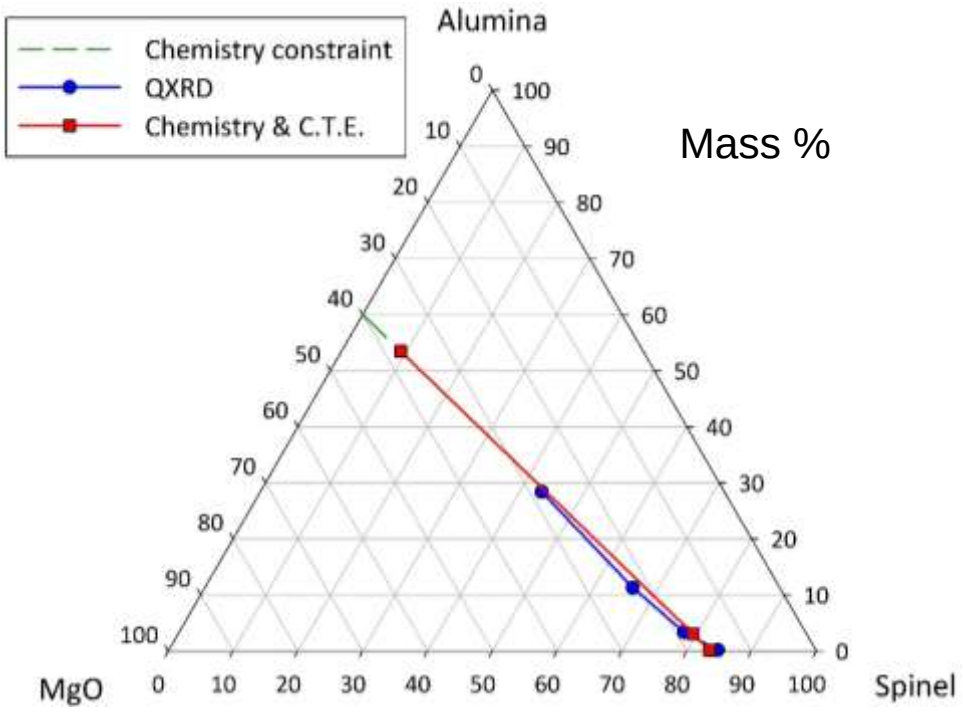

B.

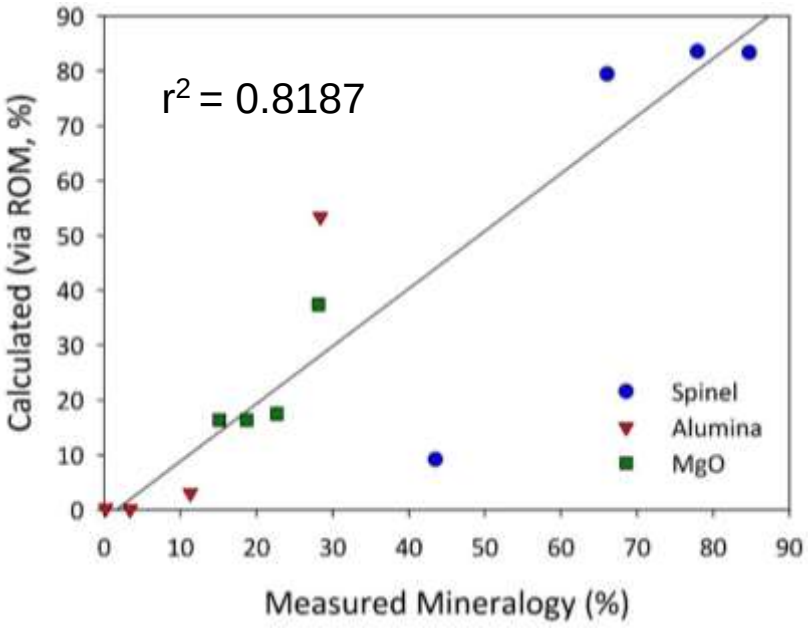

Figure 43. The mineralogy predicted from the starting chemistry and measured C.T.E. The predicted mineralogy is different from the QXRD with low $r^2 = 0.8187$.

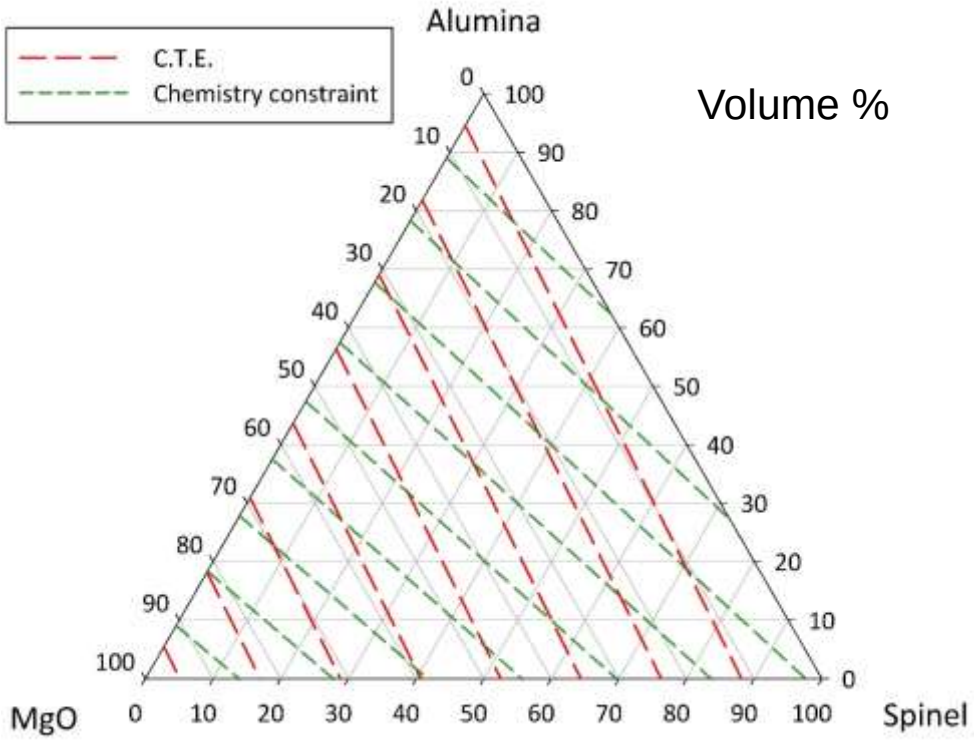

Figure 44. The grids formed by chemistry constraints and C.T.E. values increasing consistently, which disobey the second requirement of ROM approach.

SUMMARY AND CONCLUSIONS

Figure 45 compares the measured mineralogy to that predicted using ROM, incorporating density, C.T.E., and starting chemistry for all data in porcelain, mullite, and spinel systems. The mineralogy calculated via chemistry and C.T.E. in the spinel system is not considered since it disobeys the second requirement of this approach. In general this technique generates excellent agreement with the mineralogy obtained by QXRD. The results indicate that the predictions based on physical properties have an average error less than 5% compared with mineralogy data collected via QXRD.

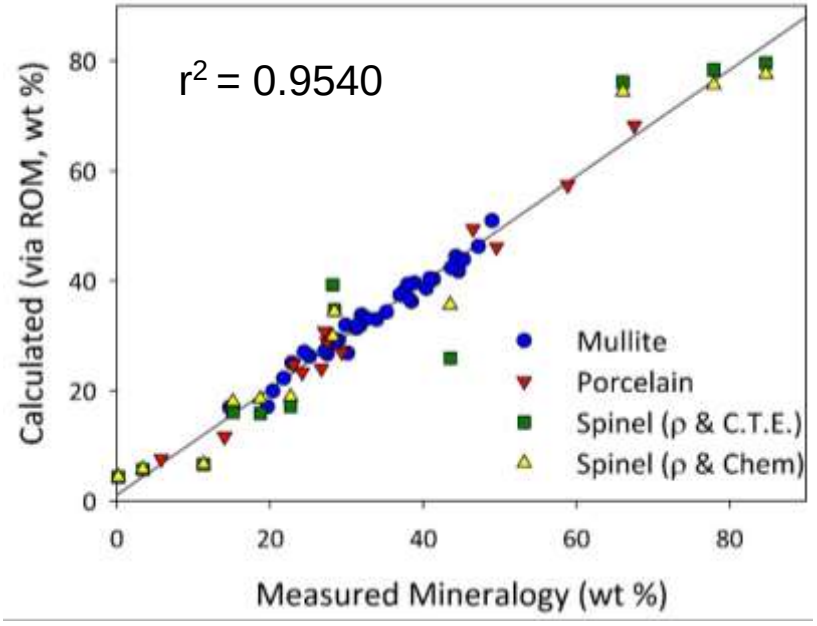

Figure 45. Comparison of measured and ROM mineralogy predictions for porcelain, mullite, and spinel systems shows a good result with an overall correlation coefficient $r^2 = 0.9540$.

The goal of this work is to demonstrate that mineralogy could be predicted by the ROM concept for a three-component system. Properties such as density and C.T.E. are selected because they are microstructure independent. The results thus demonstrate that this approach is feasible, but the samples must fulfill two basic requirements:

(1) The three components need to have significantly different property values.

(2) The properties should not increase consistently.

Chemistry constraint can be used in predicting mineralogy but also must necessarily fulfill the requirements above. Furthermore, this approach can also be used as a tool for impurity diagnosis, such as the unexpected phase, which in this case, the formation of cristobalite, can invalidate results. If the impurity levels are known, however, the ROM calculations can be corrected.

FUTURE WORK

Other materials with three components, such as Ca_2SiO_4 and $PbTiO_3$ systems, can also be analyzed through this ROM approach by either two measured properties or one property with starting chemistry. Conceptually, it should be possible to apply this technique to systems composed of more than three components, but it may be necessary to incorporate a third parameter, such as starting chemistry in a simple reaction with density and C.T.E. measurements. The calculation for multi-components materials can be extend from Equation (8):

$$\begin{bmatrix} 1 & 1 & 1 & \cdots & 1 \\ p_{a,1} & p_{a,2} & p_{a,3} & \cdots & p_{a,n} \\ p_{b,1} & p_{b,2} & p_{b,3} & \cdots & p_{b,n} \\ \vdots & \vdots & \vdots & \ddots & \vdots \\ p_{x,1} & p_{x,2} & p_{x,3} & \cdots & p_{x,n} \end{bmatrix} \begin{bmatrix} f_{1,v} \\ f_{2,v} \\ f_{3,v} \\ \vdots \\ f_{n,v} \end{bmatrix} = \begin{bmatrix} 1 \\ p_{a,m} \\ p_{b,m} \\ \vdots \\ p_{x,m} \end{bmatrix} \quad (19)$$

Where volume fraction of sample with *n* components can be predicted through *x* properties measurements.

This method is also applicable to other properties following ROM requirements. For example, elastic modulus (E) can be corrected if the volume of porosity in the sample can be measured (Equation 20).

$$\left(f_{1,v} \cdot E_1\right) + \left(f_{2,v} \cdot E_2\right) + \left(f_{3,v} \cdot E_3\right) + \cdots + \left(f_{n,v} \cdot E_n\right) + \left(f_{pores,v} \cdot 0\right) = E_S \quad (20)$$

The mechanism between C.T.E. and elastic modulus has not been well established and further study is needed in order to correct the C.T.E. from large difference in elastic modulus between components. The error of measurements also affect the result of prediction; with higher measurement reliability, the standard deviation of predicted mineralogy will be lower.

REFERENCES

1. J. R. Connolly, "Introduction to X-Ray Powder Diffraction" (2007) Accessed on: 1/1/2007. Available at <http://epswww.unm.edu/xrd/xrdclass/01-XRD-Intro.pdf>

2. C. Wong and R. S. Bollampally, "Thermal Conductivity, Elastic Modulus, and Coefficient of Thermal Expansion of Polymer Composites Filled with Ceramic Particles for Electronic Packaging," *J. Appl. Polym. Sci.,* **74** [14] 3396-403 (1999).

3. S. Torquato, "Modeling of Physical Properties of Composite Materials," *Int. J. Solids Struct.,* **37** [1] 411-22 (2000).

4. G. Y. Onoda, "Specific Volume Diagrams for Ceramic Processing," *J. Am. Ceram. Soc.,* **66** [4] 297-301 (1983).

5. K. K. Chawla, *Ceramic Matrix Composites;* pp. 134-49. Kluwer Academic Publishers, Norwell, MA, U.S.A., 1987.

6. I.-M. Low, *Ceramic-Matrix Composites: Microstructure, Properties and Applications*. CRC Press, Boca Raton, FL, U.S.A., 37-53, 2006.

7. H. T. Hahn and S. W. Tsai, *Introduction to Composite Materials*. Technomic Publishing Company, Lancaster, PA, U.S.A., 392-399, 1980.

8. C. E. Pearson, *Handbook of Applied Mathematics: Selected Results and Methods,* 2 ed., Vol. 1. Van Nostrand Reinhold, New York, NY, U.S.A., 16-20, 1983.

9. G. W. Morey, *Properties of Glass,* 2 ed.; pp. 221-94. Waverly Press, Baltimore, MD, U.S.A., 1954.

10. W. D. Kingery, *Introduction to Ceramics,* 2 ed. Wiley-Interscience New

York, NY, U.S.A., 1960.

11. E. Skovira, "Properties of the Porcelain Glass Phase"; M.S. Thesis. Alfred University, Alfred, NY, U.S.A., 2006.

12. R. C. Weast, *Handbook of Chemistry and Physics,* 50 ed. Chemical Rubber Company, Cleveland, OH, U.S.A., 1969.

13. C. Y. Ho and R. E. Taylor, *Thermal Expansion of Solids,* Vol. 4. ASM International, Materials Park, OH, U.S.A., 1998.

14. J. F. Shackelford and W. Alexander, *Materials Science and Engineering Handbook,* 3 ed. CRC Press, Boca Raton, FL, U.S.A., 2001.

15. W. M. Carty and U. Senapati, "Porcelain—Raw Materials, Processing, Phase Evolution, and Mechanical Behavior," *Journal of the American Ceramic Society,* **81** [1] 3-20 (1998).

16. W. Lerdprom, "Firing of Porcelain"; M.S. Thesis. Alfred University, Alfred, NY, U.S.A., 2014.

17. V. Colorado, "Fast Firing of Porcelain"; M.S. Thesis. Alfred University, Alfred, NY, U.S.A., 2014.

18. W. M. Carty, "Glass Phase Composition in Porcelains and Correlation with Pyroplastic Deformation"; pp. 108-32 in Vol. 24, *Whitewares and Materials.* American Ceramic Society, Westerville, OH, U.S.A., 2003.

19. K. Dana and S. K. Das, "Evolution of Microstructure in Flyash-Containing Porcelain Body on Heating at Different Temperatures," *Bull. Mater. Sci.,* **27** [2] 183-8 (2004).

20. H. Lee and W. M. Carty, *Glass Phase Composition in Porcelains and Correlation with Firing Temperature*. in Proceedings of the 106th Annual

Meeting and Exposition of the American Ceramic Society, Indianapolis, IN, U.S.A., 2004.

21. E. Rambaldi, W. Carty, A. Tucci, and L. Esposito, "Using Waste Glass as a Partial Flux Substitution and Pyroplastic Deformation of a Porcelain Stoneware Tile Body," *Ceram. Int.,* **33** [5] 727-33 (2007).

22. W. M. Carty, "Observations on the Glass Phase Composition in Porcelains"; pp. 79-94 in Vol. 23, *Materials and Equipment-Whitewares.* American Ceramic Society, Westerville, OH, U.S.A., 2002.

23. J. Anggono, "Mullite Ceramics: Its Properties Structure and Synthesis," *Jurnal Teknik Mesin,* **7** [1] 1-10 (2005).

24. C. Chen, G. Lan, and W. Tuan, "Preparation of Mullite by the Reaction Sintering of Kaolinite and Alumina," *J. Eur. Ceram. Soc.,* **20** [14] 2519-25 (2000).

25. M. Sainz, F. Serrano, J. Amigo, J. Bastida, and A. Caballero, "X-Ray Diffraction Microstructural Analysis of Mullites Obtained from Kaolinite–Alumina Mixtures," *J. Eur. Ceram. Soc.,* **20** [4] 403-12 (2000).

26. C. Baudin, R. Martínez, and P. Pena, "High‐Temperature Mechanical Behavior of Stoichiometric Magnesium Spinel," *Journal of the American Ceramic Society,* **78** [7] 1857-62 (1995).

27. K. Mackenzie, J. Temuujin, T. Jadambaa, M. Smith, and P. Angerer, "Mechanochemical Synthesis and Sintering Behaviour of Magnesium Aluminate Spinel," *J. Mater. Sci.,* **35** [22] 5529-35 (2000).

28. J. Martín‐Márquez, A. G. De la Torre, M. A. Aranda, J. M. Rincón, and M. Romero, "Evolution with Temperature of Crystalline and Amorphous

Phases in Porcelain Stoneware," *J. Am. Ceram. Soc.,* **92** [1] 229-34 (2009).

29. S. Somiya, R. F. Davis, and J. Pask, *Mullite and Mullite Matrix Composites;* pp. 221-9. American Ceramic Society, Westerville, OH, U.S.A., 1990.

30. S. T. Lundin, *Studies on Triaxial Whiteware Bodies*. Almqvist & Wiksell, Stockholm, Sweden, 1959.

31. J. E. Shelby, *Introduction to Glass Science and Technology*. The Royal Society of Chemistry, Cambridge, England, 1997.

APPENDIX

A. Porcelain System

Table VI. Quantitative X-Ray Diffraction Data in Porcelain System

Temperature (°C)	Mullite (Wt. %)	St. Dev.	Quartz (Wt. %)	St. Dev.	Glass (Wt. %)	St. Dev.
1200	24.16	0.36	29.34	0.72	46.50	1.08
1300	27.40	0.61	23.04	0.19	49.56	0.42
1400	27.12	0.10	14.04	0.39	58.84	0.50
1500	26.68	0.93	5.77	0.11	67.55	0.95

Table VII. Predicted Mineralogy in Porcelain System

Temperature (°C)	Mullite (Wt. %)	St. Dev.	Quartz (Wt. %)	St. Dev.	Glass (Wt. %)	St. Dev.
1200	23.42	0.28	27.08	0.58	49.50	0.38
1300	28.96	0.24	24.83	0.45	46.22	0.31
1400	30.83	0.19	11.71	0.37	57.46	0.25
1500	24.08	0.22	7.63	0.32	68.28	0.26

Table VIII. Properties measurements in Porcelain System

Temperature (^oC)	Ave. Density (g/cm^3)	St. Dev.	Ave. C.T.E. ($x10^{-6}/K$)	St. Dev.
1200	2.6097	0.0012	9.6776	0.1345
1300	2.6427	0.0012	9.3225	0.1045
1400	2.6188	0.0009	6.9309	0.0868
1500	2.5609	0.0013	6.1818	0.0717

Table IX. Properties Calculated through ROM in Porcelain System

Temperature (^oC)	Ave. Density (g/cm^3)	St. Dev.	Ave. C.T.E. ($x10^{-6}/K$)	St. Dev.
1200	2.6213	0.0046	10.1029	0.1376
1300	2.6265	0.0038	8.9772	0.0283
1400	2.5993	0.0018	7.3347	0.0713
1500	2.5735	0.0064	5.8567	0.0198

B. Mullite System

Table X. Quantitative X-Ray Diffraction Data in Mullite System

Sample	Temperature (°C)	Mullite (Wt. %)	St. Dev.	Corundum (Wt. %)	St. Dev.	Glass (Wt. %)	St. Dev.
AE42	1200	25.14	0.20	31.22	0.36	43.65	0.38
AE42	1250	25.60	0.22	31.54	0.22	41.05	0.57
AE42	1300	27.01	0.82	31.41	0.50	37.40	1.72
AE42	1350	27.41	0.59	32.53	0.37	36.63	0.61
AE42	1400	30.09	0.60	31.90	0.26	37.95	0.76
AE42	1450	37.22	0.89	28.91	0.60	33.87	1.47
AE42	1500	44.58	0.49	22.83	0.23	32.59	0.27
AE52	1200	20.34	1.17	38.83	0.34	40.83	1.19
AE52	1250	20.65	0.81	39.35	1.03	38.50	1.54
AE52	1300	21.31	0.30	40.48	0.81	33.88	0.77
AE52	1350	23.11	0.19	40.55	1.45	32.92	0.44
AE52	1400	24.45	0.25	40.38	0.49	35.17	0.68
AE52	1450	29.85	0.58	38.44	0.23	31.71	0.79
AE52	1500	44.23	0.26	28.32	0.88	27.46	0.63
AE62	1200	14.70	0.38	47.19	0.97	38.11	1.34
AE62	1250	16.04	0.18	47.73	0.03	35.28	0.49
AE62	1300	16.61	0.55	48.16	0.56	32.02	0.40
AE62	1350	17.80	0.96	49.18	0.53	31.02	1.26
AE62	1400	19.66	0.40	48.98	0.55	31.37	0.17
AE62	1450	27.64	1.01	45.23	0.78	27.13	0.75
AE62	1500	41.31	0.87	36.93	0.34	21.76	0.97

Table XI. Predicted Mineralogy in Mullite System

Sample	Temperature (°C)	Mullite (Wt. %)	St. Dev.	Corundum (Wt. %)	St. Dev.	Glass (Wt. %)	St. Dev.
AE42	1200	31.76	4.77	27.94	2.96	40.30	1.83
AE42	1250	11.15	0.15	41.08	0.07	47.76	0.11
AE42	1300	-0.27	3.76	48.43	2.34	51.84	1.42
AE42	1350	2.84	5.01	47.47	3.11	49.68	1.93
AE42	1400	31.94	3.41	30.62	2.12	37.44	1.30
AE42	1450	42.11	2.18	26.54	1.36	31.35	0.82
AE42	1500	46.07	0.43	22.40	0.18	31.53	0.35
AE52	1200	25.23	3.20	36.32	1.99	38.45	1.21
AE52	1250	18.19	1.29	41.78	0.79	40.03	0.52
AE52	1300	-16.85	4.08	64.47	2.54	52.38	1.54
AE52	1350	-1.67	4.31	56.50	2.69	45.17	1.63
AE52	1400	31.48	3.02	35.86	1.87	32.66	1.17
AE52	1450	36.06	2.05	33.66	1.28	30.28	0.78
AE52	1500	47.93	4.37	26.65	2.73	25.42	1.65
AE62	1200	21.72	4.56	43.31	2.84	34.97	1.72
AE62	1250	11.24	0.86	51.63	0.52	37.13	0.37
AE62	1300	-5.24	5.08	62.42	3.16	42.82	1.94
AE62	1350	-2.23	3.47	61.99	2.16	40.24	1.31
AE62	1400	21.27	0.39	48.38	0.22	30.35	0.21
AE62	1450	32.45	2.30	41.69	1.43	25.86	0.87
AE62	1500	43.16	2.82	35.65	1.76	21.19	1.07

Table XII. Properties Measurements in Mullite System

Sample	Temperature (^oC)	Ave. Density (g/cm^3)	St. Dev.	Ave. C.T.E. ($x10^{-6}/K$)	St. Dev.
AE42	1200	2.9451	0.0038	5.4768	0.0992
AE42	1250	2.9495	0.0014	5.8184	0.0024
AE42	1300	2.9529	0.0001	6.0101	0.0788
AE42	1350	2.9670	0.0042	5.9878	0.1048
AE42	1400	2.9858	0.0018	5.5481	0.0720
AE42	1450	3.0194	0.0007	5.4408	0.0466
AE42	1500	2.9943	0.0035	5.3315	0.0060
AE52	1200	3.0083	0.0016	5.7000	0.0681
AE52	1250	3.0244	0.0022	5.8470	0.0272
AE52	1300	3.0374	0.0003	6.4557	0.0879
AE52	1350	3.0604	0.0001	6.2488	0.0935
AE52	1400	3.0606	0.0032	5.6922	0.0652
AE52	1450	3.0706	0.0008	5.6335	0.0446
AE52	1500	3.0767	0.0010	5.4440	0.0954
AE62	1200	3.0819	0.0014	5.8962	0.0994
AE62	1250	3.1102	0.0022	6.1285	0.0183
AE62	1300	3.1185	0.0033	6.5060	0.1120
AE62	1350	3.1420	0.0013	6.4224	0.0772
AE62	1400	3.1589	0.0018	6.0491	0.0078
AE62	1450	3.1635	0.0007	5.8635	0.0516
AE62	1500	3.1739	0.0011	5.6959	0.0635

Table XIII. Properties Calculated through ROM in Mullite System

Sample	Temperature (^oC)	Ave. Density (g/cm^3)	St. Dev.	Ave. C.T.E. ($x10^{-6}/K$)	St. Dev.
AE42	1200	2.9330	0.0051	5.5613	0.0095
AE42	1250	2.9401	0.0049	5.7887	0.0231
AE42	1300	2.9486	0.0081	6.0748	0.1203
AE42	1350	2.9691	0.0109	6.0165	0.0587
AE42	1400	2.9875	0.0083	5.5899	0.0071
AE42	1450	3.0092	0.0171	5.5036	0.0163
AE42	1500	2.9869	0.0013	5.3430	0.0060
AE52	1200	3.0003	0.0115	5.7655	0.0096
AE52	1250	3.0095	0.0171	5.9668	0.0534
AE52	1300	3.0300	0.0107	6.3529	0.0360
AE52	1350	3.0491	0.0223	6.2470	0.0727
AE52	1400	3.0627	0.0094	5.8144	0.0144
AE52	1450	3.0849	0.0090	5.7643	0.0071
AE52	1500	3.0667	0.0112	5.4890	0.0239
AE62	1200	3.0742	0.0186	6.0003	0.0295
AE62	1250	3.0948	0.0022	6.1389	0.0572
AE62	1300	3.1049	0.0065	6.4436	0.0079
AE62	1350	3.1345	0.0134	6.3246	0.0329
AE62	1400	3.1522	0.0051	6.0642	0.0163
AE62	1450	3.1781	0.0008	5.9718	0.0258
AE62	1500	3.1761	0.0112	5.7320	0.0103

C. Spinel Synthesis

Table XIV. Quantitative X-Ray Diffraction Data in Spinel System

Temperature (°C)	Spinel (Wt. %)	St. Dev.	Alumina (Wt. %)	St. Dev.	MgO (Wt. %)	St. Dev.
1450	43.48	1.76	28.37	1.01	28.16	0.76
1500	66.05	0.98	11.30	0.10	22.65	1.08
1550	77.93	1.00	3.37	0.12	18.71	1.12
1600	84.72	0.51	0.17	0.02	15.11	0.51

Table XV. Predicted Mineralogy (by Density and C.T.E.) in Spinel System

Temperature (°C)	Spinel (Wt. %)	St. Dev.	Alumina (Wt. %)	St. Dev.	MgO (Wt. %)	St. Dev.
1450	25.96	2.04	34.72	1.07	39.32	1.75
1500	76.15	1.42	6.64	0.89	17.21	1.13
1550	78.41	1.19	5.69	0.54	15.90	1.05
1600	79.60	2.71	4.33	2.25	16.08	1.70

Table XVI. Predicted Mineralogy (by Chemistry and Density) in Spinel System

Temperature (°C)	Spinel (Wt. %)	St. Dev.	Alumina (Wt. %)	St. Dev.	MgO (Wt. %)	St. Dev.
1450	35.65	1.69	34.45	1.21	29.90	0.48
1500	74.38	1.40	6.69	1.00	18.93	0.40
1550	75.67	0.85	5.77	0.61	18.56	0.24
1600	77.60	3.55	4.38	2.54	18.01	1.00

Table XVII. Predicted Mineralogy (by Chemistry and C.T.E.) in Spinel System

Temperature (°C)	Spinel (Wt. %)	St. Dev.	Alumina (Wt. %)	St. Dev.	MgO (Wt. %)	St. Dev.
1450	9.17	6.21	53.42	4.45	37.40	1.76
1500	79.46	4.33	3.06	3.10	17.49	1.23
1550	83.55	4.05	0.12	2.90	16.33	1.15
1600	83.36	6.51	0.26	4.66	16.38	1.84

Table XVIII. Properties Measurements in Spinel System

Temperature (^oC)	Ave. Density (g/cm^3)	St. Dev.	Ave. C.T.E. ($x10^{-6}/K$)	St. Dev.
1450	3.7092	0.0044	10.1333	0.1379
1500	3.6112	0.0035	8.6486	0.0871
1550	3.6080	0.0021	8.5664	0.0811
1600	3.6033	0.0087	8.5704	0.1302

Table XIX. Properties Calculated through ROM in Spinel System

Temperature (^oC)	Ave. Density (g/cm^3)	St. Dev.	Ave. C.T.E. ($x10^{-6}/K$)	St. Dev.
1450	3.6872	0.0034	9.4186	0.0514
1500	3.6269	0.0006	8.9978	0.0638
1550	3.5997	0.0006	8.7244	0.0657
1600	3.5891	0.0001	8.4963	0.0301